AD-A184 350 THERMOPLASTIC ELASTOMERS AS LOVA (LOW VULNERBBILITY AMMUNITION) BINDERS(U) MASSACHUSETTS UNIV AMHERST J C CHIEN ET AL 1986 N00014-85-K-0888 1/1

UNCLASSIFIED F/G 19/1 NL

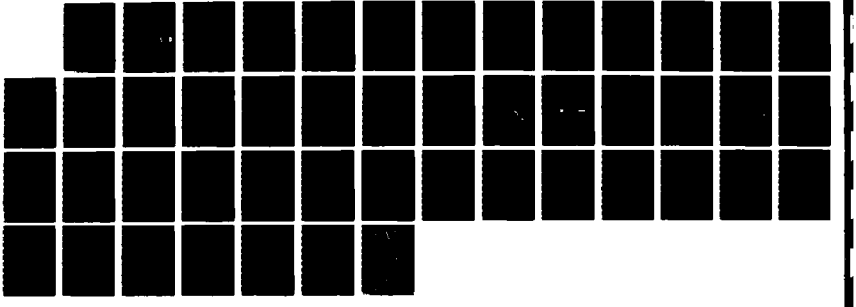

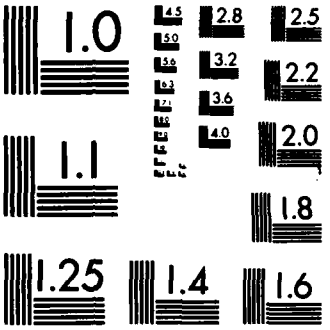

University of Massachusetts
Office of Grants and Contract Administration
Munson Hall
Amherst, MA 01003

(12)

ANNUAL REPORT

Project: Thermoplastic Elastomers as LOVA Binders

Contract No.: N00014-85-K-0880

Period of Report: Jan. 1986 to Dec. 1986

Principal Investigators: Professor James C.W. Chien
Professor Richard J. Farris
Professor C. Peter Lillya
Professor H.H. Winter

Postdoctoral Fellows: K.F. Angeung
R. Zhou
D. Ng
Y.G. Cheun
B. Xu
Z.S. Cheng

Ph.D. Candidates: C.F. Chu,
D.T. Hsieh
J.L. Hong
N. Goldberg
T.S. Stephens
K.H. Wei
L.L. Anderson
E. Kolb

Ph.D. degrees granted: J.L. Hong
C.F. Chu,
K.H. Wei
N. Goldberg

Publications:

Structure Property Relationships in Thermoplastic Elastomers: III. Segmented Polyacetal-Polyurethanes, B. Xu, D.N. Khanna, C.P. Lillya and J.C.W. Chien, J. Appl. Polym. Sci., 31, 123 (1986).

Simulation of Welding Flows in a Slit. Part I: Kinematics, K.H. Wei, M.F. Malone and H.H. Winter, Polym. Eng. Sci., 26, 1012-1019 (1986).

Structure-Property Relatinships in Thermoplastic Elastomers III. Segmented Polyacetal-Polyurethanes, B. Xu, D.N. Khanna, C.P. Lillya and J.C.W. Chien, J. Appl. Polym. Sci., 31, 123 (1986).

Equibiaxial Extension of Two Polymer Melts: Polystyrene and Low Density Polyethylene, P.R. Soskey and H.H. Winter, J. Rheol., 24, 493 (1985).

Acidolysis of Poly(4-Methyl-1,3,-dioxolane), M.A. Diab, D.T.

Hseih, C.P. Lillya and J.C.W. Chien, submitted

Acid Catalyzed Degradation of Poly(2-butyl-1,3,6-trioxocane), B. Xu, C.P. Lillya and J.C.W. Chien, submitted.

Cationic Polymerization of 1,3,6-Trioxocane and 2-Butyl-1,3,6-trioxocane, B. Xu, C.P. Lillya and J.C.W, Chien, submitted.

Technical Reports Issued:

Acidolysis of Poly(4-methyl-1,3-dioxolane), #12, January 10, 1986.

Acid-Catalyzed Degradation of Poly(2-butyl-1,3,6-trioxocane), #13, January 10, 1986.

Relaxation Properties of Some Segmented Polyurethane-$CaCO_3$ Composites. A Dielectric Study, #14, May 8, 1986.

Model for Prediction of the Elastic Response of Composite Materials over Wide Ranges of Concentration, #15, May 8, 1986.

Structure-Property Relationships in Thermoplastic Elastomers III. Segmented Polyacetal-Polyurethanes, #16, June 9, 1986.

TABLE OF CONTENTS

I. SYNTHESIS

A. Liquid Crystalline TPE

1. From promesogens - Conventional mesogenic compounds have high T_m which limits the conditions for processing. In this work, low melting promesogens were used to synthesize liquid crystalline compounds and polymers.

Alkyl-4(4'-alkoxybenzoyloxy)benzoates (with C_1-C_{10} alkyl and alkoxy groups) are monotropic compounds which melt directly to isotropic liquids. Twin liquid crystalline compounds, TLCC, of alkoxybenzoyloxybenzoic acid have been synthesized. The TLCC with methoxy end groups and trioxyethylene spacer is weakly mesogenic; but replacement of the methoxy with an n-butoxy end group results in a smectic mesophase. With the decamethylene spacer, the TLCC with a methoxy end group shows a nematic mesophase whereas the compound with n-butoxy end groups exhibits both smectic and nematic mesophases. The latter has much higher ordered liquid crystalline states than the former. The polymeric TLCC with n-butoxy end groups and $\bar{M}_n$ = 650 poly-THF spacers display significant liquid crystalline order. It is suggested that the microphase separation due to dissimilar solubility parameters can be an important contributing factor toward mesophase formation.

2. From mesogens - Azo and azoxy aromatic systems are currently being investigated to test the feasibility of this project.

4,4-Azoxy benzoic acid has been prepared by a reduction of p-nitrobenzoic acid with sodium hydroxide in methanol. This purified material was then converted to the diacid chloride by treatment with thionyl chloride. The azoxy benzoyl chloride was purified by recrystallization in good yields.

4,4'-Azobenzoic acid has been prepared by a reductive coupling with sodium hydroxide in methanol in the presence of zinc powder. This material was isolated, characterized and converted to the diacid chloride.

The following materials have also been prepared to: a) further characterize the azo and azoxy monomers, and b) to prepare other related mesogens for the polymerization study.

These materials are:

1) 3,3'-dimethyl-4,4'-azoxybenzoic acid
2) p-nitrosobenzoic acid
3) 3,3'-dimethyl-4,4'-azo ethyl benzoate
4) azo-4-benzoic acid-4'-ethylbenzoate
5) 3 methyl 4,4'-azoethylbenzoate

All these materials have been characterized by infrared analysis, melting point and ^{1}H NMR spectroscopy.

The polymerization of the azo and azoxy monomers has enjoyed only limited success. Both materials have been reacted with poly propylene oxide molecular weight (MW) 425 and with polytetrahydrofuran MW 650.

A variety of reaction conditions have been investigated, of

which polymerization in tetrachloroethane with 1.5 mole excess of pyridine seems to be the most fruitful. The polymer resulting from these reactions form weak rubbery materials.

B. Acid Sensitive LOVA Hard Segments

Poly(1,3-dioxolane-co-trioxocane), poly(DT), were found to have demonstrable acid catalyzed depolymerizability. The copolymer has T_m's ranging from 30° to 179°C depending upon comonomer composition. For DOD needs, the ideal T_m should be in the 80° to 100° range. This would permit fast and safe manufacturing of propellents. Poly(DT)'s have been synthesized with a range of comonomer feed ratios. It was found that poly(DT) obtained with comonomer feed composition of 35 mole % trioxocane and 65 mole % of dioxolane has T_m of 90 - 92°C; it has T_m = 86 - 88°C with 30/70 mole % feed of trioxocane/dioxolane.

The DSC curves for the poly(DT)'s are shown in Figures 1 and 2. There are some low melting fractions which begins to melt between 60° to 65°. Two methods have been used to fractionate poly(DT). In the first method 20% of poly(DT) was dissolved in tetrachloroethane/THF followed by methanol precipitation (50%) and solvent removal (30%). In the second method acetone/methanol was used to separate two equal weight fractions. Neither method affected any separation; the fractions have broader range of T_m.

The low melting fraction must be due to copolymers richer in dioxolane because this monomer polymerizes more rapidly than trioxocane. Sharp melting poly(DT) can be synthesized if this

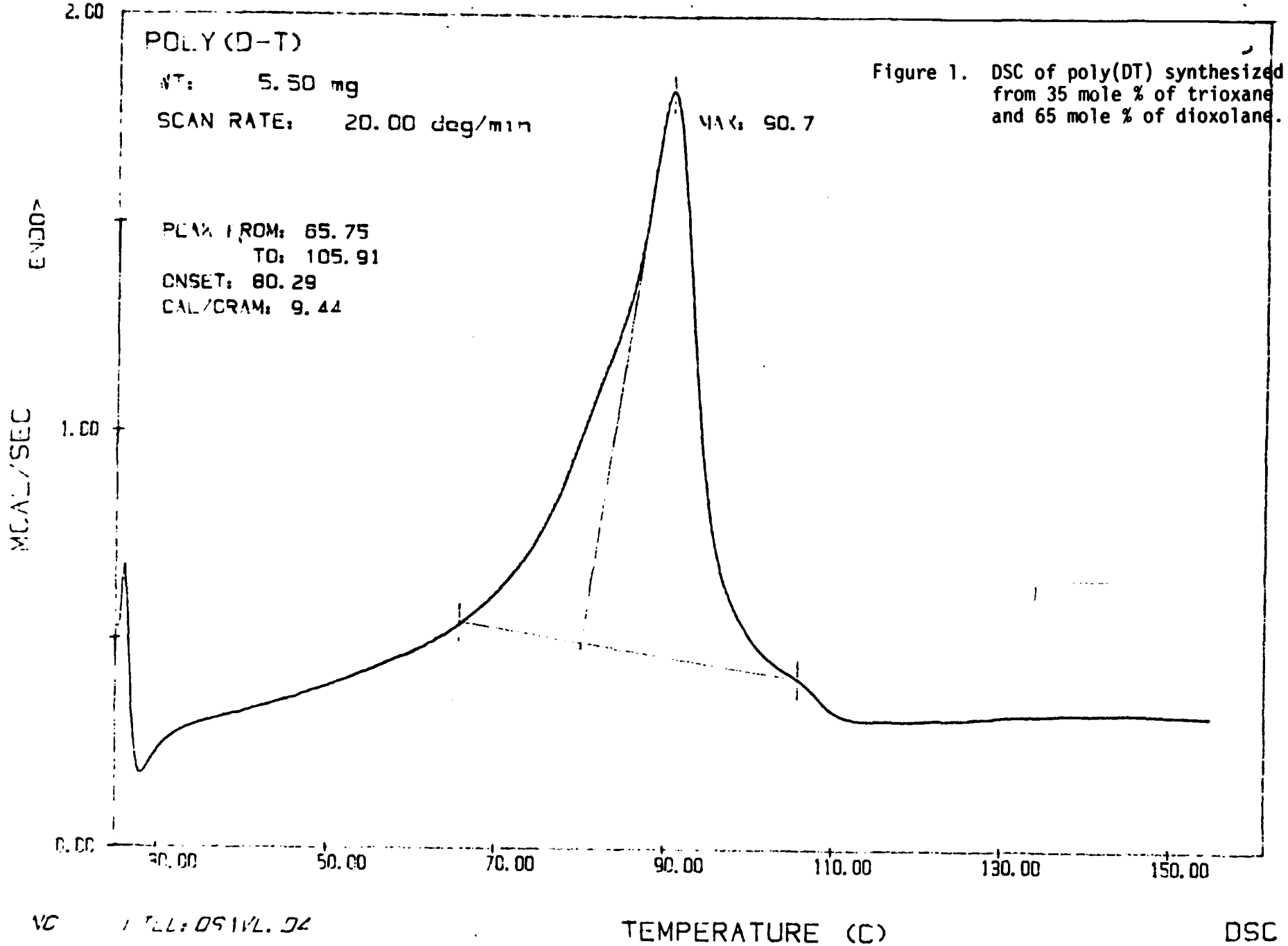

Figure 1. DSC of poly(DT) synthesized from 35 mole % of trioxane and 65 mole % of dioxolane.

VC [illegible]

DATE: 86/12/13 TIME: 23:16

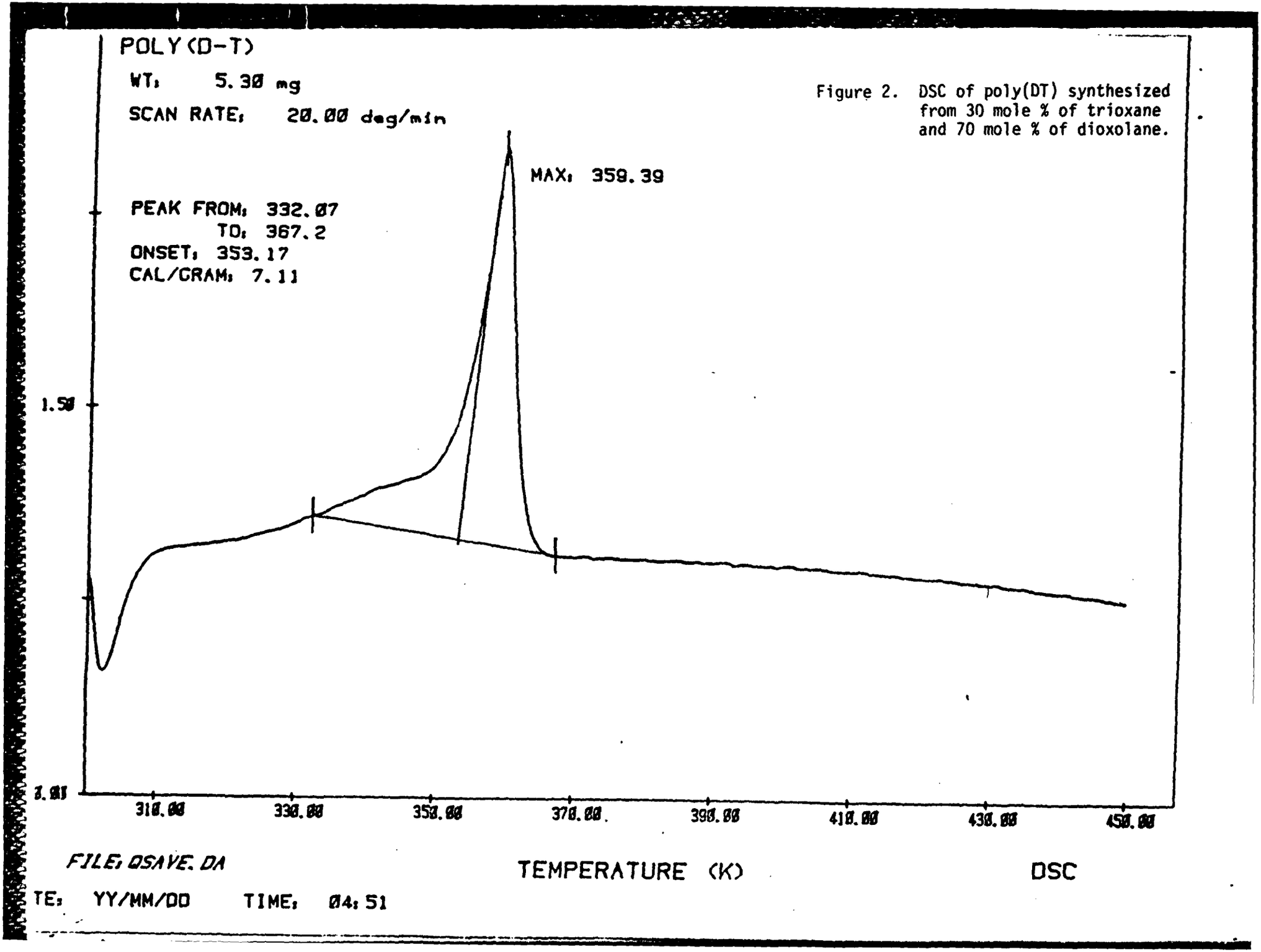

Figure 2. DSC of poly(DT) synthesized from 30 mole % of trioxane and 70 mole % of dioxolane.

composition drift can be eliminated which may be achievable by continuous copolymerization process. Alternatively, one can begin a batch copolymerization richer in trioxocane and adding dioxolane as reaction proceeds.

C. Cationic Polymerizations of Trioxocane and 2-butyltrioxocane.

The polymerization of 1,3,6-trioxocane (TOC) has been reinvestigated. The reaction occurs without an induction period to give high MW linear polymers. The degree of polymerization is not independent of conversion. Polymers having $\bar{M}_n$ as high as 81,000 and $\bar{M}_w/\bar{M}_n$ ~ 1.4 and with good mechanical strength can be obtained. These results contrast with earlier reports of long induction periods and products with $\bar{M}_n$ ~ 5,000. Substituents at the 2 position greatly reduces the polymerizability of dioxolane and dioxepanes. It is therefore a significant result that 2-butyl-1,3,6-trioxocane (2-Bu-TOC) is readily polymerized and at a slightly faster rate than polymerization of TOC under identical conditions. The $\bar{M}_n$ of poly(2-Bu-TOC) increases monotonically with conversion reaching a value of 7,700. The thermodynamic parameters for the polymerizations of both systems have been obtained. There is strong argument in favor of the open chain alkoxycarbenium ion as the propagating species for trioxocane polymerizations over the cyclic oxonium ion.

D. Cationic Polymerization of 2-butyl dioxepane

The polymerization of 2-butyl dioxepane (2-bu-DOX) have been studied from -20° to 10°C in 1,2-dichloroethane initiated by $BF_3 \cdot Et_2O$. The $\bar{M}_n$ increases from 6000 at 10° to 8600 at -20° with the same $\bar{M}_w/\bar{M}_n$ of 1.4 to 1.5. ^1H and ^{13}C NMR and IR showed the ring opening to occur between the acetal oxygen and substituted carbon atoms and the polymer contains alternating tetrahydrofuran and valeraldehyde units. From the equilibrium monomer concentrations the following thermodynamic parameters were obtained for the polymerization: $\Delta H^\circ_{ss} = -7.3 \pm 1.2$ kJ mole^{-1} and $\Delta S^\circ_{ss} = -32.9 \pm 6.5$ J(mol K)$^{-1}$. The ceiling temperature at 1 M monomer concentration is -51°C.

E. Poly(1,3-dioxepane) Polyurethane

Poly(1,3-dioxepane) was prepared by 1,3-dioxepane monomer, using 1,4-butanediol as chain transfer agent to control molecular weight, and using sulfuric acid as catalyst. Molecular weight was determined by Karl-Fisher method.

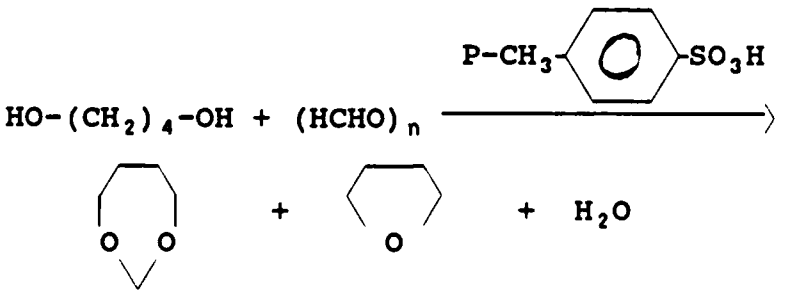

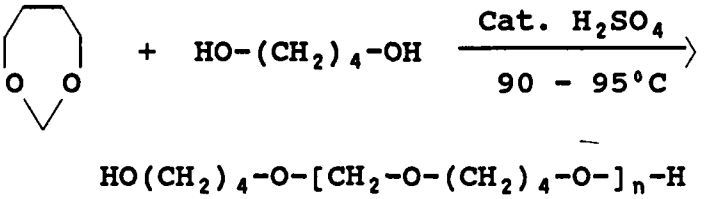

$$\text{HO}(\text{CH}_2)_4\text{-O-}[\text{CH}_2\text{-O-}(\text{CH}_2)_4\text{-O-}]_n\text{-H}$$

Aliphatic chain extenders were prepared from trans amidation to obtain the dihydroxyethylamide of dicarboxylic acid with n = 0 to 8

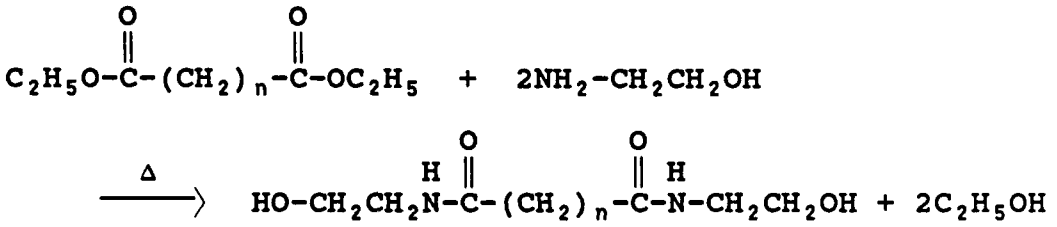

About 50 polyurethanes were prepared from the poly(DOX), the above chain extenders and using isophorone diisocyanate, MDI and TDI coupling agents. The purposes here were to find effects of the amide group and methylene length of the chain extender and the symmetry of diisocyanates (IDI, TDI, asymmetric; MDI symmetric) on crystallinity, T_g, and mechanical properties of the polyurethanes. The findings can be summarized as follows.

(a) Polyurethanes prepared from chain extender without amide groups and asymmetric diisocyanates are viscous liquids.

(b) Polyurethane prepared as in (a) but with amide groups are TPE's but exhibit no melting or crystallization phenomenon associated with poly(DOX).

(c) Substitution of MDI for the asymmetric diisocyanate in (b) forms TPE's with melting/crystallization of poly(DOX) by low temperature DSC.

(d) The T_g of the poly(DOX) polyurethanes are not affected by any structural variations mentioned above.

(e) The mechanical properties are dependent on hard segment contents with greater elastic moduli, longer elongation, and greater tensile strength at break with higher hard segment content.

Acidolysis of poly(DOX) with 0.25% p-toluene sulfonic acid was studied under isothermal conditions. The results shown in Figure 3 are as expected. The activation energy was 17 kcal mol^{-1}.

II. Rheology

A. Rheology of Highly Filled Polymer Melts

The flow behavior of polymeric liquids containing high concentrations of particulate solids is dominated by two phenomena, deformation history dependence and boundary layer formation. At low flow rates, or small deformations, the stress in a filled polymer melt depends on the entire history of the deformation (Figure 4).

For small deformations, rheological properties may be measured in a parallel plate rheometer (see Figure 5). Dynamic moduli are defined for oscillatory shear by:

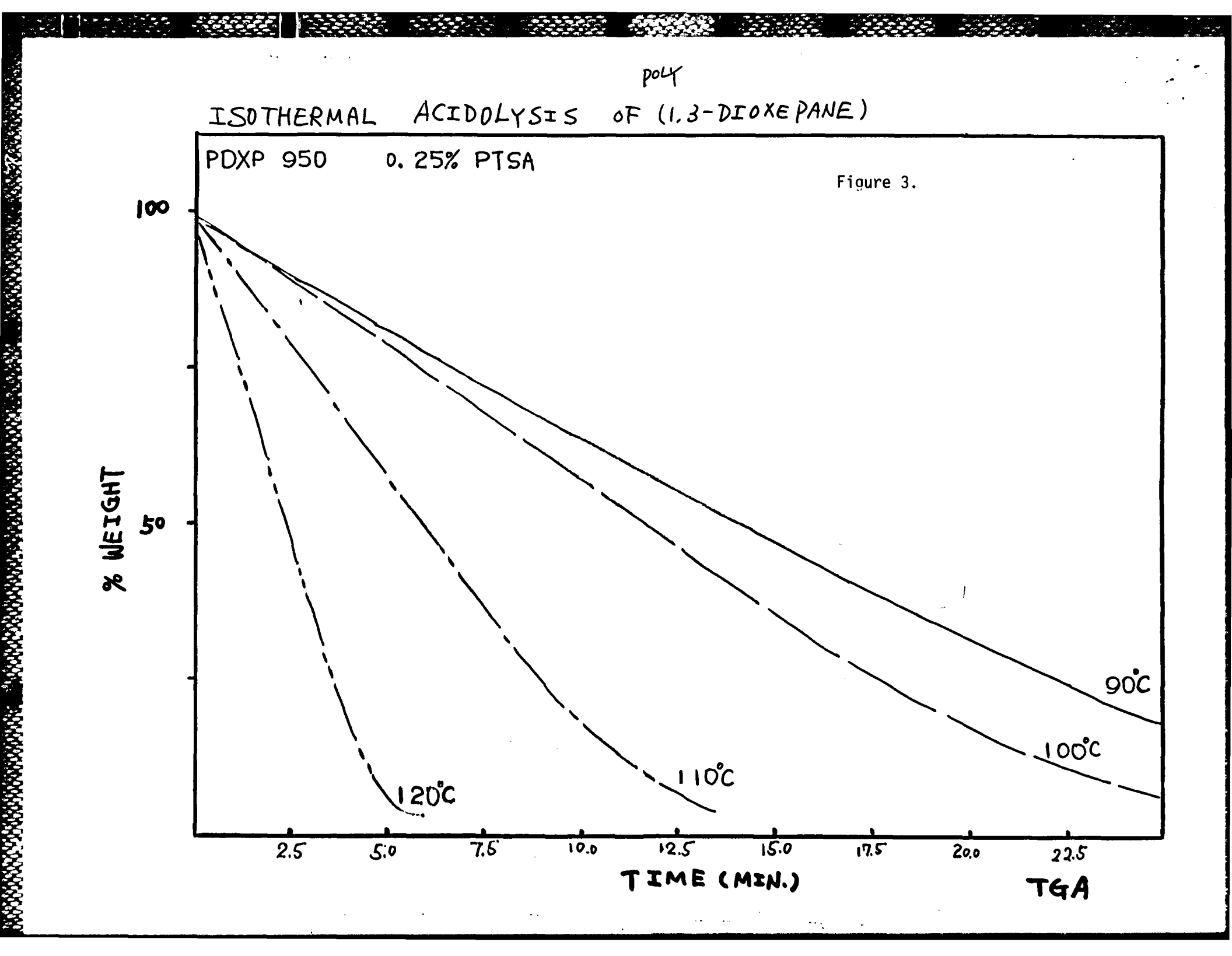
POLY
ISOTHERMAL ACIDOLYSIS OF (1,3-DIOXEPANE)
PDXP 950 0.25% PTSA
Figure 3.
100
50
% WEIGHT
90°C
100°C
110°C
120°C
2.5
5.0
7.5
10.0
12.5
15.0
17.5
20.0
22.5
TIME (MIN.)
TGA

Figure 4

Rheology of filled polymers and unfilled polymers

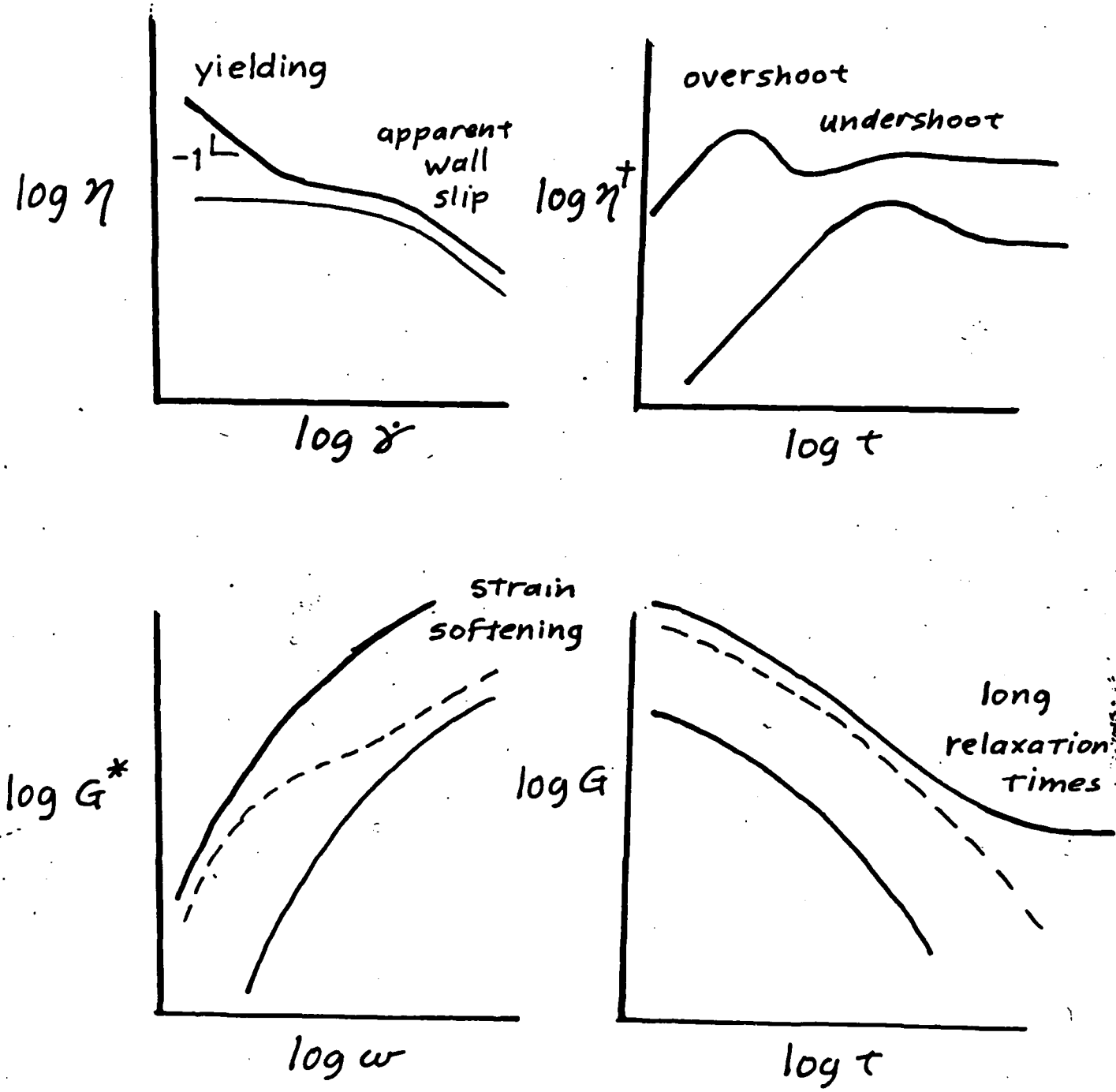

Figure 5

cone & plate

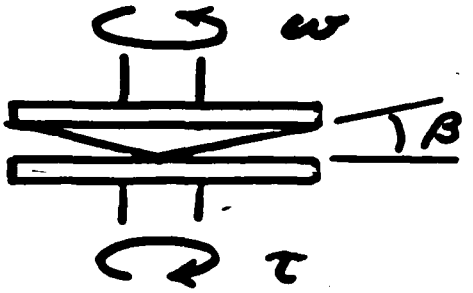

parallel plates

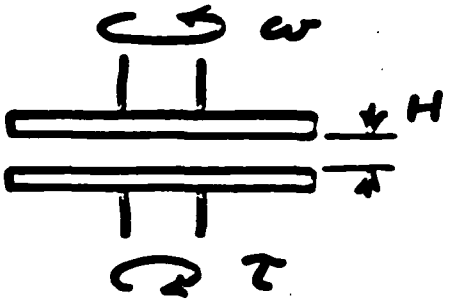

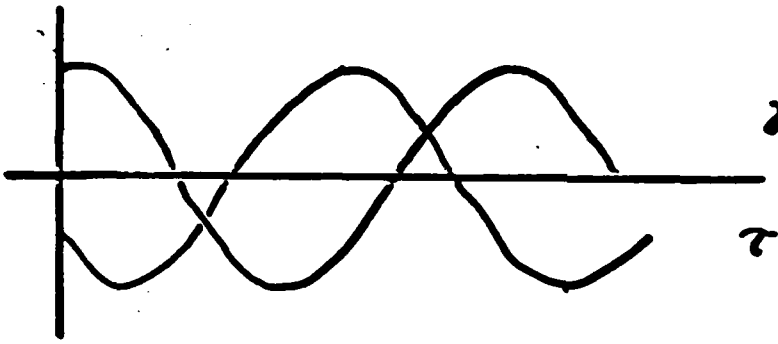

$$\dot{\gamma} = \dot{\gamma}_0 \cos \omega t$$

$$\tau = \eta' \dot{\gamma}_0 \cos \omega t + \eta'' \dot{\gamma}_0 \sin \omega t$$

$G'' = \omega \eta'$, loss modulus

$G' = \omega \eta''$, storage modulus

$\eta^* = \sqrt{(\eta')^2 + (\eta'')^2}$, complex viscosity

$$\tau(t) = G'(\omega)\ \gamma_0\ \sin(\omega t) + G''(\omega)\ \gamma_0\ \cos(\omega t)$$

where

$$\gamma(t) = \gamma_0\ \sin(\omega t)$$

and

G' = storage modulus

G'' = loss modulus

γ = shear strain

In Figure 6, the dynamic moduli of a 50 vol % $CaCO_3$ (Georgia Marble Gamasperse 6541, 1 - 10 μm) filled poly(dimethylsiloxane) at an angular frequency of 10.0 radian/s for the strain amplitude history shown in Figure 7. The moduli decay quickly upon the application of a oscillatory shear strain of amplitude 0.1 and increase slowly when the strain amplitude is decreased to 0.01. Repeatedly increasing and decreasing the strain amplitude causes the dynamic moduli to decrease and increase, but they approach different values each time. The stress response of the material to small deformations depends on deformations occurring far in the past. The material has very long relaxation times and is strain softening. In Figure 8, the complex modulus of the same material is shown as a function of strain amplitude. The modulus decreases with increasing strain for strain amplitudes as low as

Figure 6

PDMS / $CaCO_3$, 45 vol % $CaCO_3$

30 °C

rate = 10. rad/s, strain = 1%, 10%

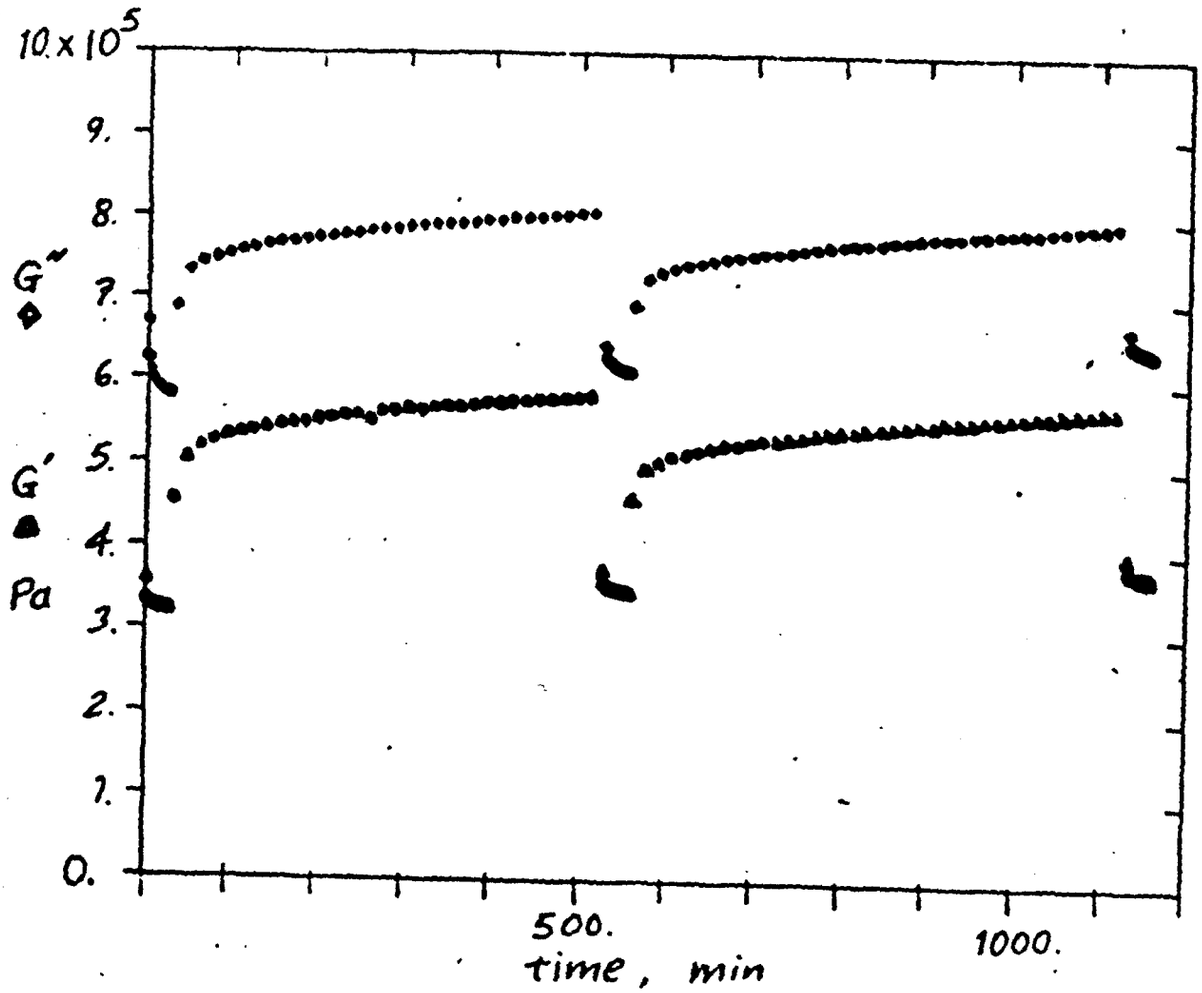

Figure 7

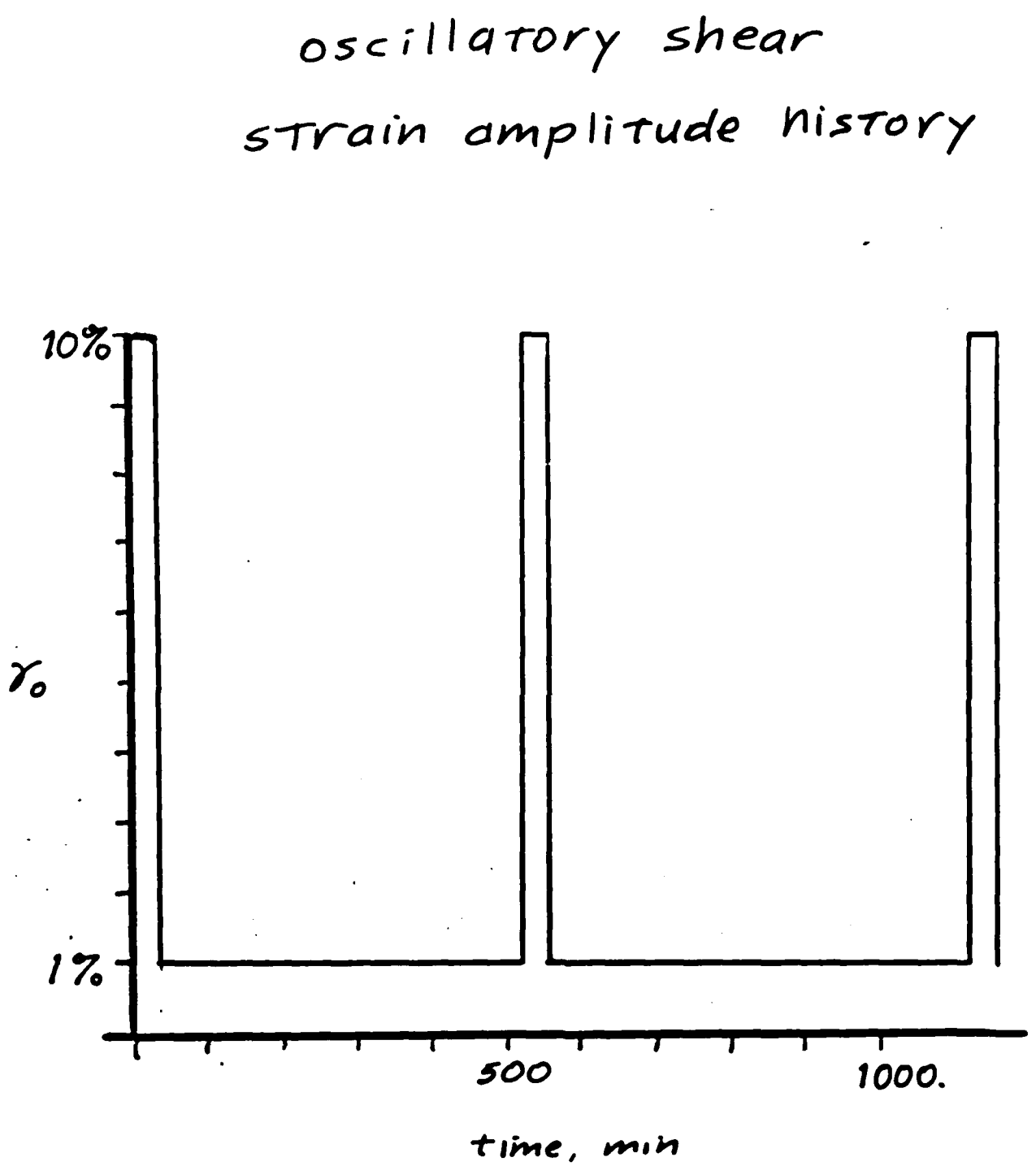
oscillatory shear
strain amplitude history
10%
γ_o
1%
500
1000.
time, min

Figure 8

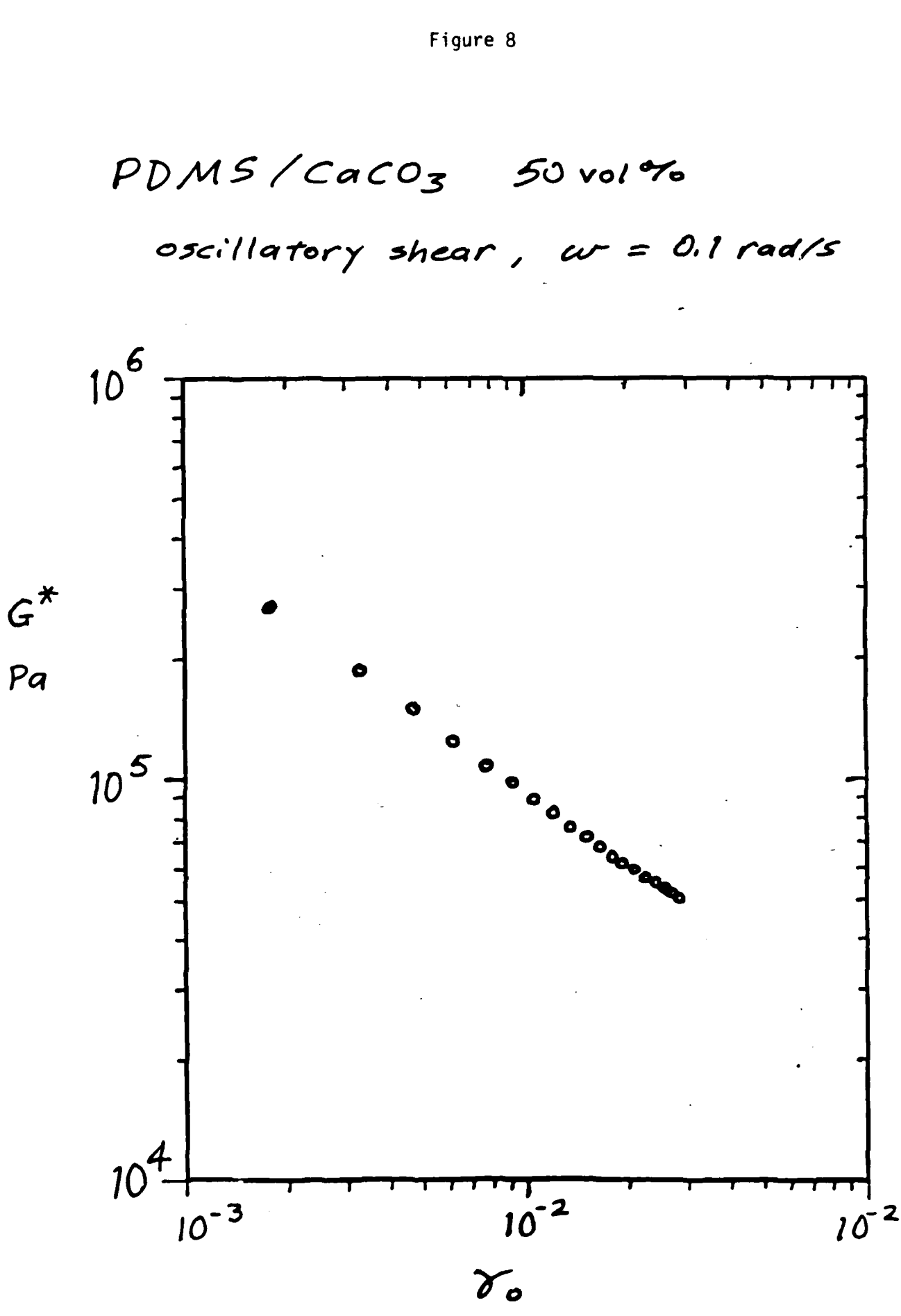
PDMS / CaCO3 50 vol %
oscillatory shear, ω = 0.1 rad/s
10^6
10^5
10^4
G*
Pa
10^-3
10^-2
10^-2
γ0

0.0003. Strain softening is also seen in step shear strain (Figure 9).

Strain softening is seen for the $CaCO_3$ filled PDMS in extensional flow. Equibiaxial extension is created in lubricated squeezing flow (Figure 10) (Soskey and Winter, 1985). The transient elongational viscosity of the PDMS/$CaCO_3$ depends on the extension rate, even at short times (Figure 11) as compared with unfilled polymer melts, for which the transient elongational viscosity is independent of the rate at short times (Figure 12). In step elongational strain, the filled PDMS is very susceptible to strain softening (Figure 13).

At high flow rates, rheological properties may be measured in a capillary rheometer (see Figures 14, 15, and 16). The shear stress at the capillary wall is related to the pressure gradient down the capillary:

$$\tau_R = \frac{R}{2}\frac{dP}{dL}$$

The apparent shear rate is defined:

$$\bar{\gamma}_a = \frac{4Q}{\pi R^3}$$

For simple materials which do not slip at walls, the relation between the wall shear stress and the apparent shear rate contains the same information as the relation between the shear

Figure 9

PDMS / $CaCO_3$ 50 vol %

step shear strain

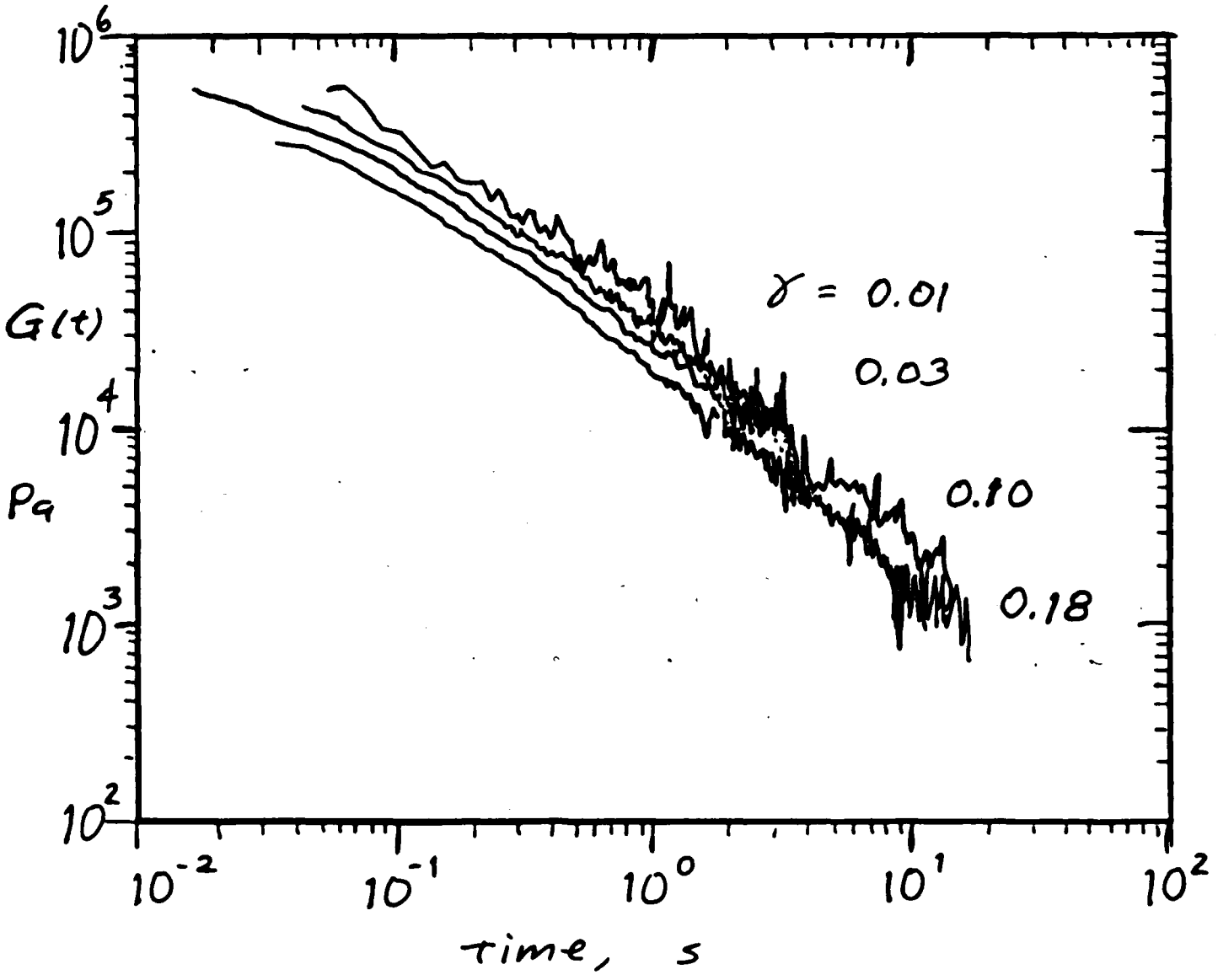

Figure 10

Lubricated Squeeze Flow

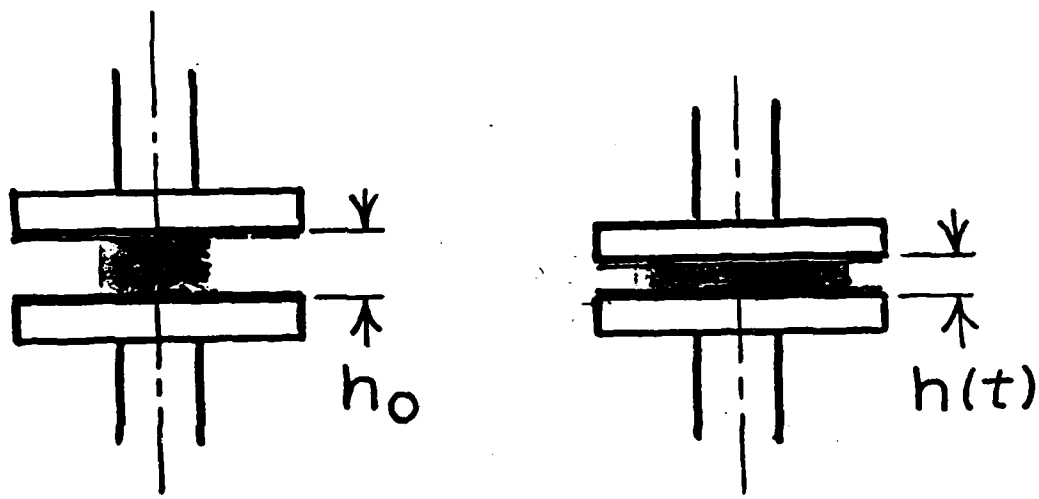

$$\varepsilon_B = \frac{1}{2} \ln \left(\frac{h_o}{h(t)} \right)$$

$$\dot{\varepsilon}_B = -\frac{1}{2} \frac{1}{h(t)} \frac{dh(t)}{dt}$$

Figure 11

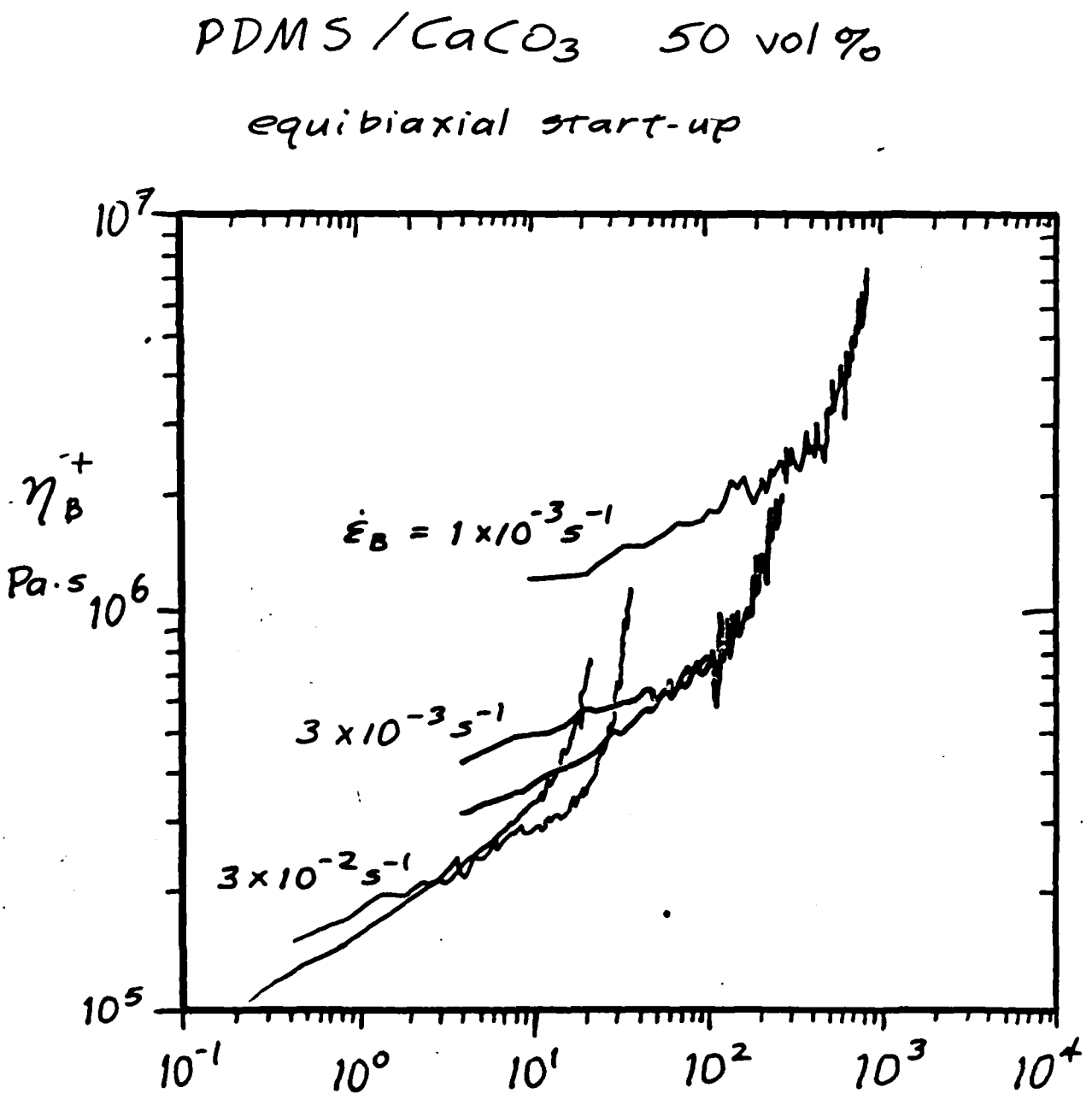
PDMS / CaCO3 50 vol %
equibiaxial start-up
η_B^{-+}
Pa·s
10^7
10^6
10^5
$\dot{\varepsilon}_B = 1 \times 10^{-3} s^{-1}$
$3 \times 10^{-3} s^{-1}$
$3 \times 10^{-2} s^{-1}$
10^{-1}
10^0
10^1
10^2
10^3
10^4

Figure 12

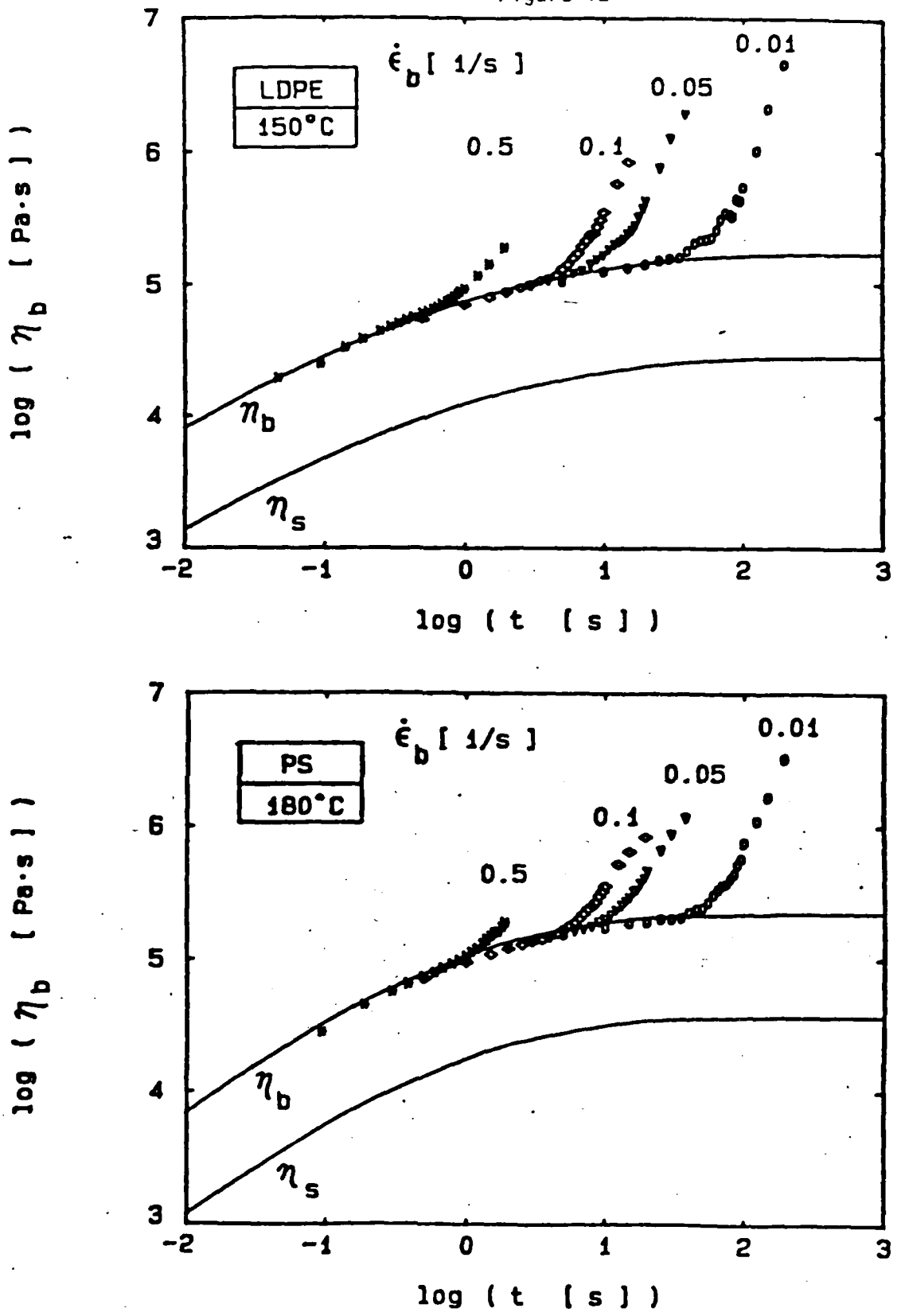

Transient equibiaxial extensional viscosity measured with RDS-LA utilizing changing area lubricated squeezing technique.
a) LDPE, T = 150°C
b) PS, T = 180°C
The linear viscoelastic limit for start-up in shear (lower solid line) and in extension (upper solid line) is calculated from data of Table I.

(Soskey and Winter, 1985)

Figure 13

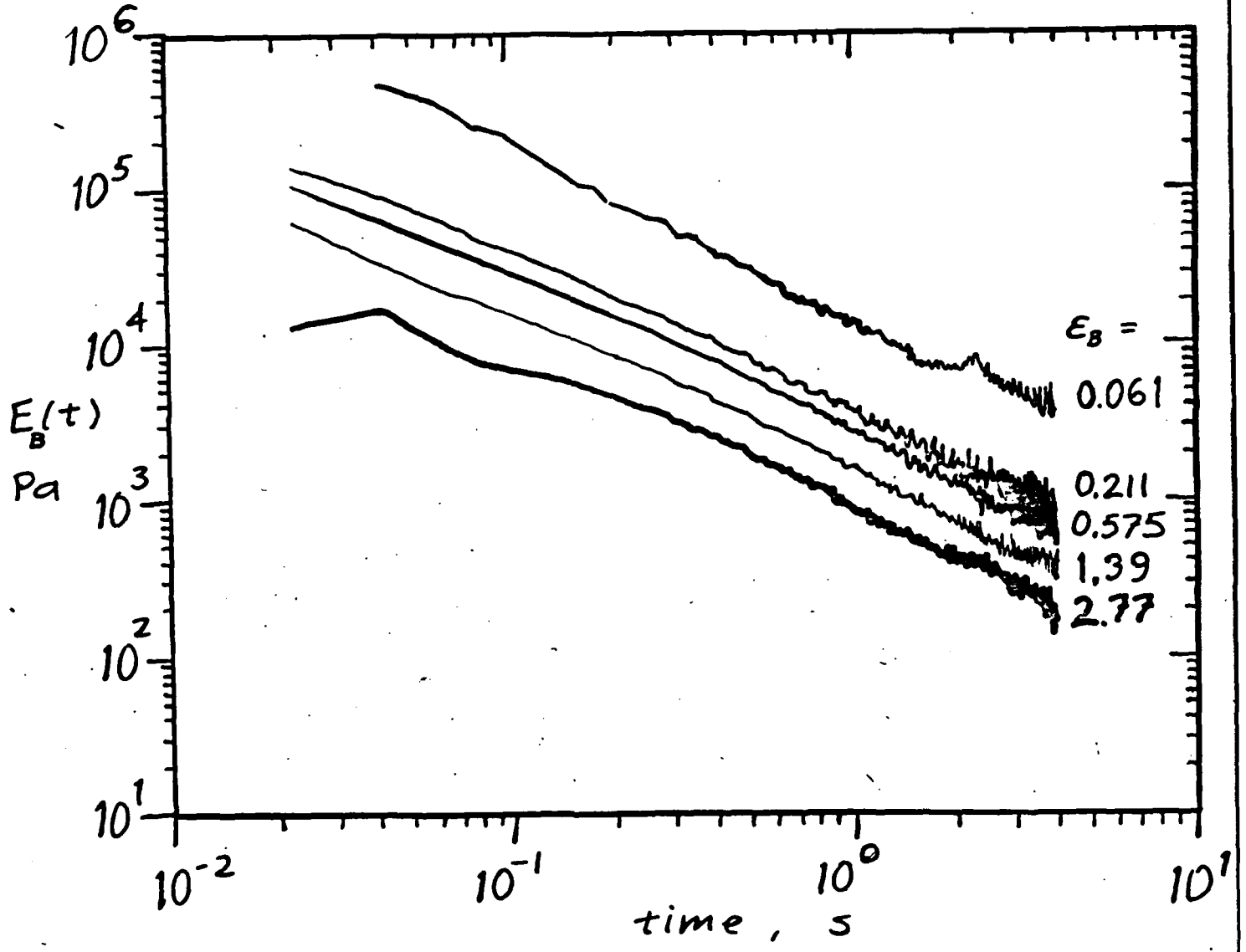
PDMS / CaCO3 45 vol %
step strain, equibiaxial extension
10^6
10^5
10^4
10^3
10^2
10^1
E_B(t)
Pa
10^-2
10^-1
10^0
10^1
time, s
ε_B =
0.061
0.211
0.575
1.39
2.77

Figure 14

flow through a capillary

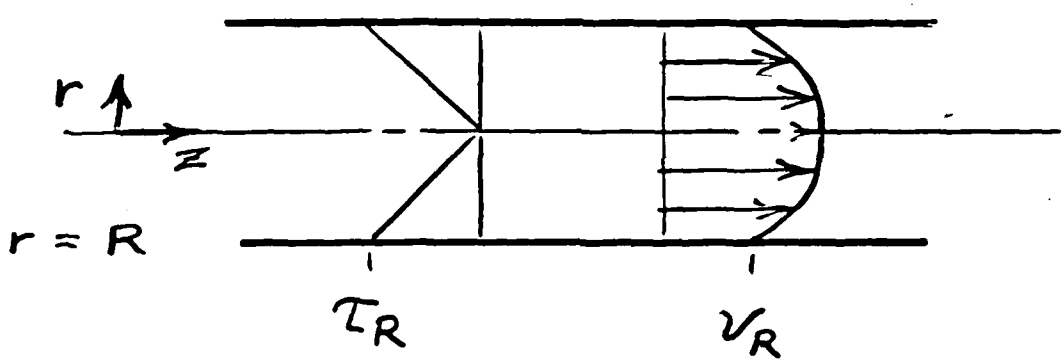

$$\tau_R = \frac{R}{2}\left(\frac{\partial P}{\partial z}\right) \qquad \dot{\gamma}_a = \frac{4Q}{\pi R^3}$$

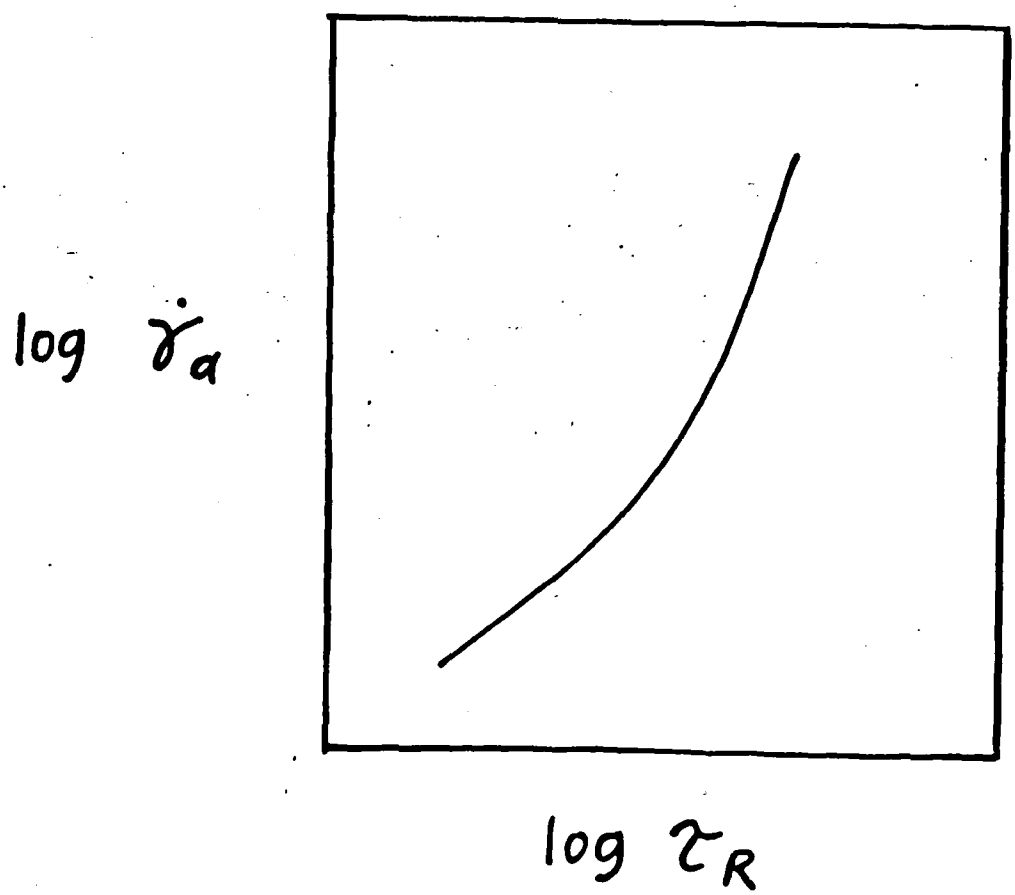

Figure 15

$$\tau = \frac{r}{2}\left(\frac{\partial P}{\partial z}\right)$$

$$\tau_R = \frac{R}{2}\left(\frac{\partial P}{\partial z}\right) = \frac{R}{2}\frac{\Delta P}{L}$$

$$Q = 2\pi \int_0^R r v \, dr$$

$$Q = 2\pi \left[\frac{v r^2}{2}\Big|_0^R - \int_0^R \frac{r^2}{2} dv \right]$$

at $r = R$, $v = v_R$

$$Q = \pi \left[v_R R^2 - \int_0^R r^2 \left(\frac{\partial r}{\partial r}\right) dr \right]$$

$$\tau = \left(\frac{r}{R}\right)\tau_R$$

$$r = \frac{R\tau}{\tau_R}$$

$$dr = \frac{R}{\tau_R} d\tau$$

$$\frac{\partial v}{\partial r} = -\dot{\gamma}$$

$$Q = \pi v_R R^2 + \frac{\pi R^3}{\tau_R^3} \int_0^{\tau_R} \tau^2 \dot{\gamma} \, d\tau$$

$$\dot{\gamma}_a = \frac{4Q}{\pi R^3} = \frac{4 v_R}{R} + \frac{4}{\tau_R^3} \int_0^{\tau_R} \tau^2 \dot{\gamma} \, d\tau$$

Figure 16

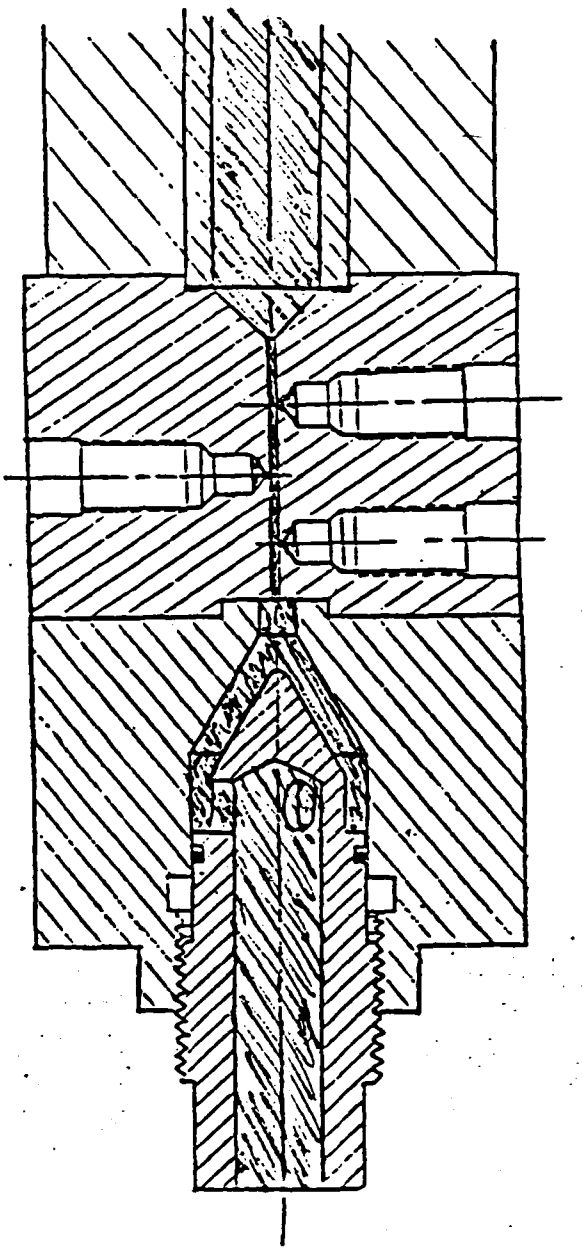

Capillary rheometer with pressure control valve.

viscosity and the shear rate. For materials which slip at the capillary wall, the apparent shear rate is not uniquely related to the wall shear stress, but is given by:

$$\gamma_a = \frac{4v_R}{R} + \frac{4}{\tau_R^3}\int^{\tau R} \tau^2\dot{\gamma}d\tau$$

Figures 17 and 18 show the apparent shear rate for a range of wall shear stresses which were measured for a $CaCO_3$ (OMYA FT 2 - 6 μm) filled PDMS in capillaries of radius 1.588 mm and 0.794 mm. At low apparent shear rates, the apparent shear rate is independent of the capillary radius, but at high rates, the dependence on radius is very large. The apparent shear rates measured in the two capillaries can differ by a factor of 10 at a given wall shear stress.

Figures 19 and 20 show the flow curves for $CaCO_3$ (OMYA F 2 - 6 μm) filled PDMS measured in the same two capillaries. The $CaCO_3$ in this sample has a similar particle size distribution, but has no surface treatment. The flow curves for this sample show a larger radius dependence at high apparent shear rates. This large dependence on the capillary radius cannot be accounted for by wall slip alone. For a material which slips at the wall, the largest radius dependence of the apparent shear rate can be R^{-1}. This implies that for a two-fold increase in the radius, wall slip can cause at most a two-fold decrease in the apparent

Figure 17

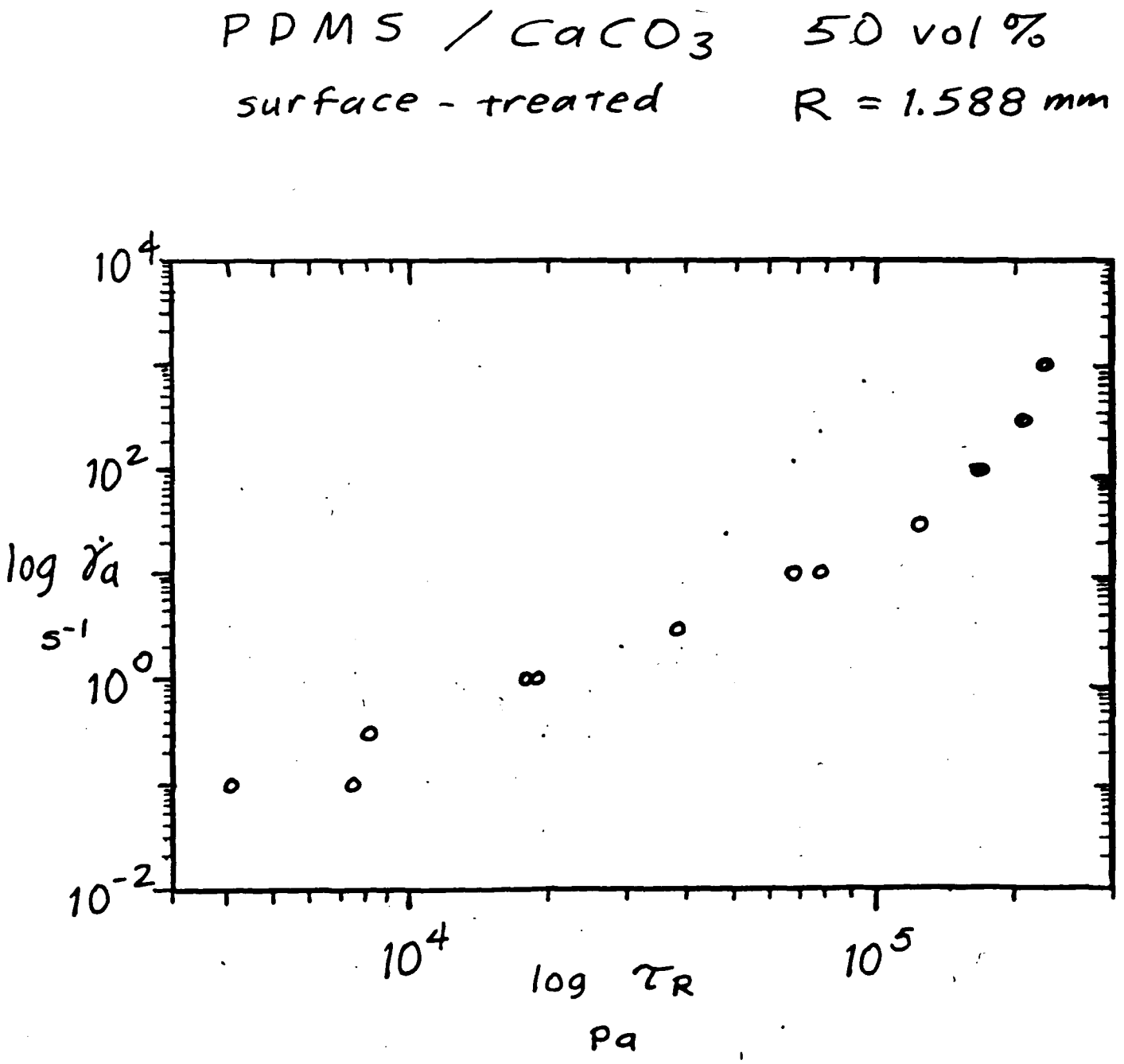
PDMS / CaCO3 50 vol %
surface - treated R = 1.588 mm
10^4
10^2
10^0
10^-2
log γ̇a
s^-1
10^4
log τR
10^5
Pa

Figure 19

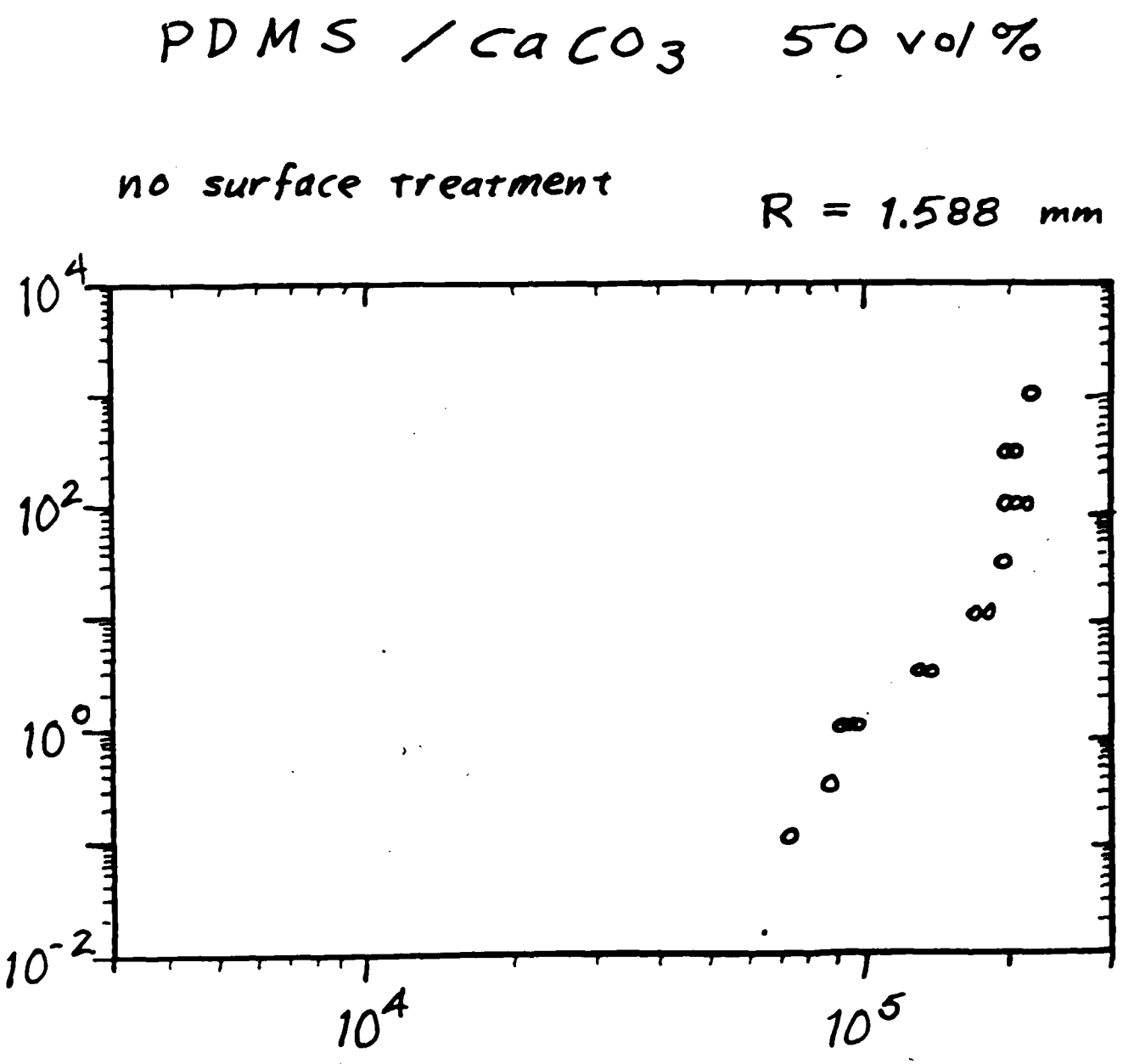
PDMS / CaCO3 50 vol %
no surface treatment
R = 1.588 mm
10^4
10^2
10^0
10^-2
10^4
10^5

Figure 18

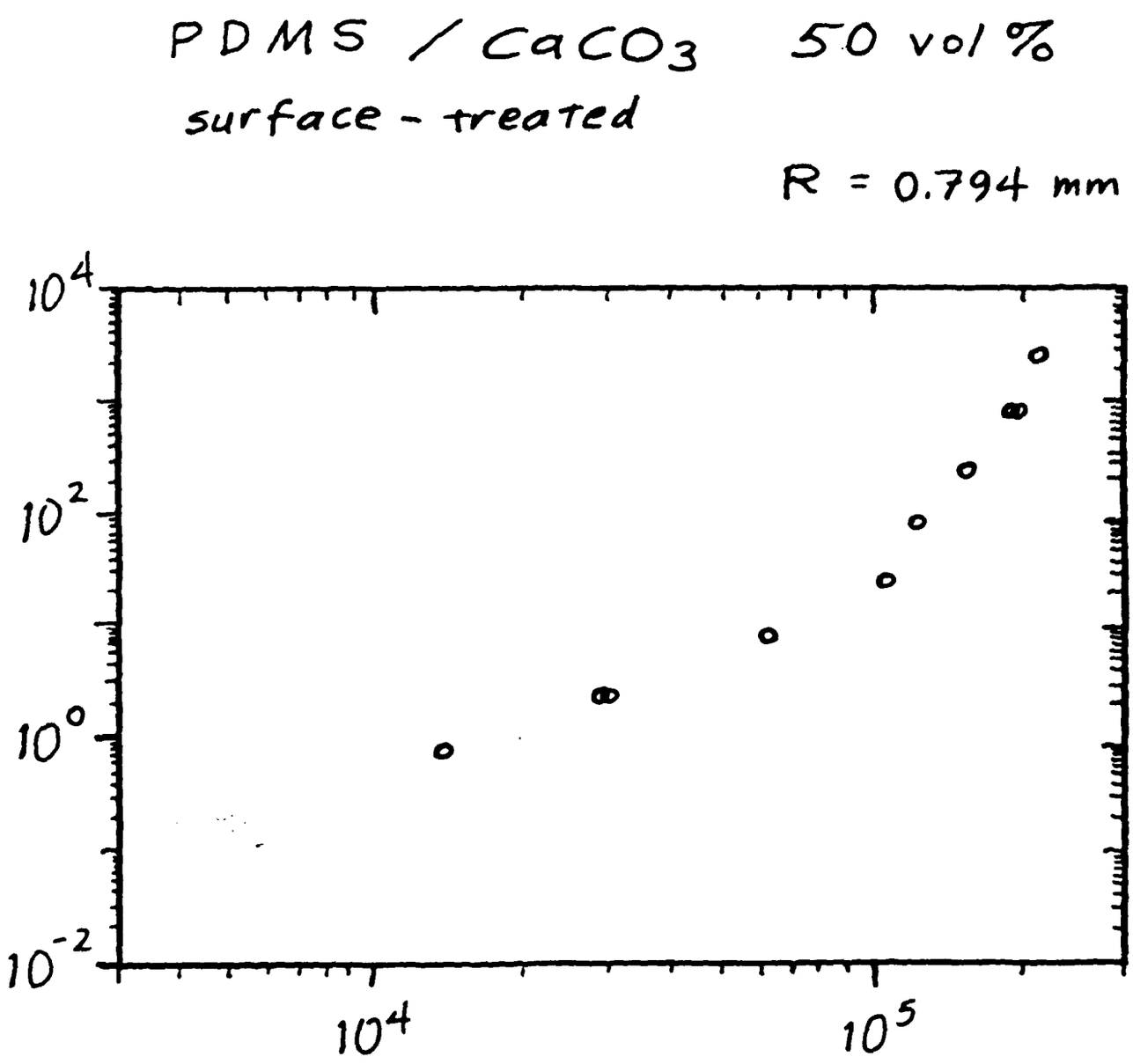
PDMS / CaCO3 50 vol %
surface - treated
R = 0.794 mm
10^4
10^2
10^0
10^-2
10^4
10^5

Figure 20

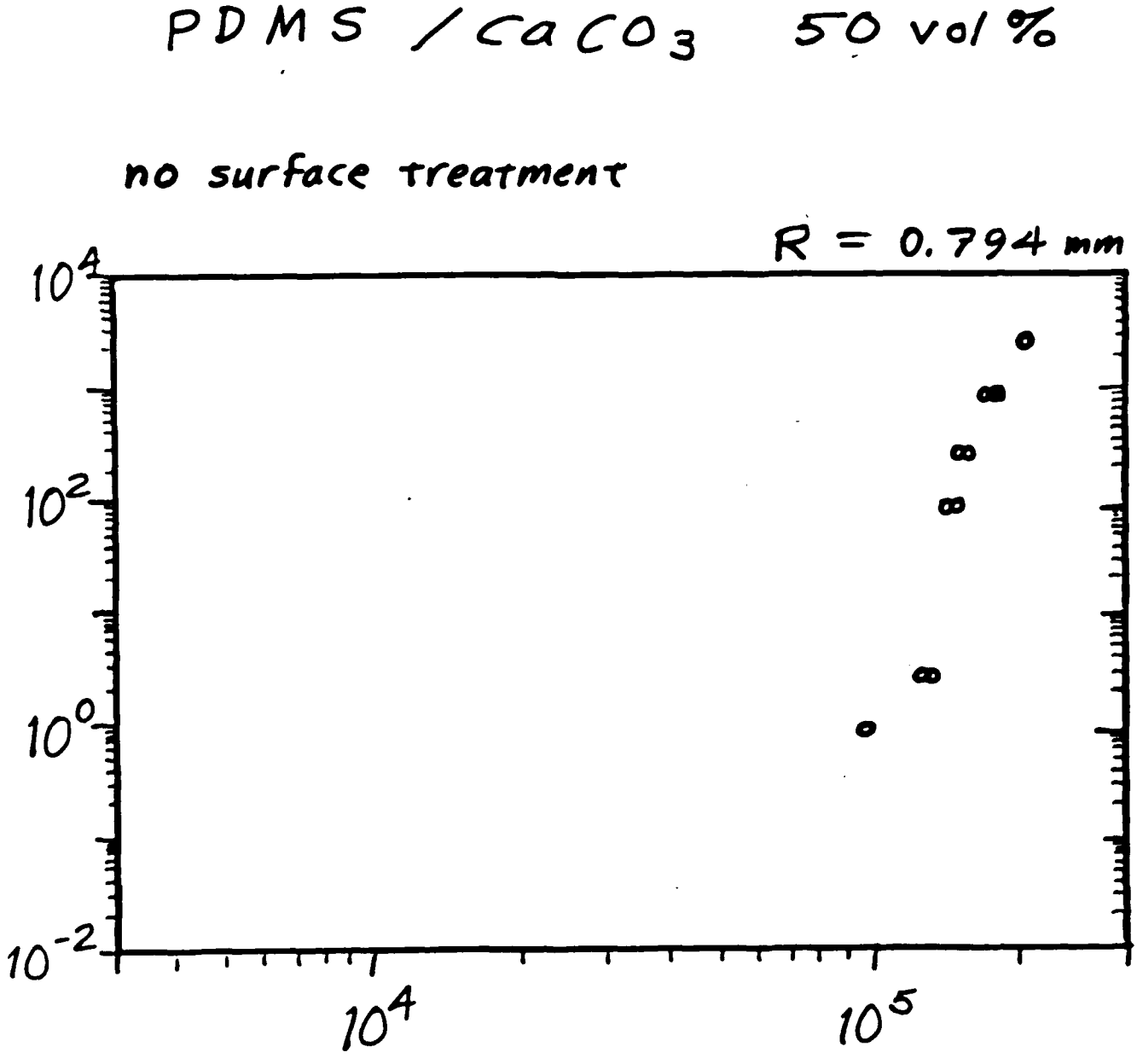
PDMS / CaCO3 50 vol %
no surface treatment
R = 0.794 mm
10^4
10^2
10^0
10^-2
10^4
10^5

shear rate. A much larger decrease is observed for the $CaCO_3$ filled PDMS.

It is believed that this severe radius dependence can be accounted for by the presence of a boundary layer. If a layer forms at the wall with different rheological properties than the material remote from the wall, then a large radius dependence can result. For example, let us assume there exists a layer of thickness δ at the wall of a capillary with a different viscosity function than the material in the interior of the capillary, and that the thickness of this layer is independent of the capillary radius. If the two viscosity functions are described by the power law, then the flow curves may be calculated explicitly (see Figures 21 and 22). When the power law index of the boundary layer is smaller than that of core, the flow curve will depend strongly on the radius at high stresses. When the power law index of the layer is greater than that of the core, radius dependence is seen at low stresses (see Figure 20). Figure 24 shows the flow curves for a particular choice of the parameters for comparison with the flow curves measured for the PDMS filled with the surface-treated $CaCO_3$ (OMYA FT). A large radius dependence is seen at high apparent shear rates, however, this simple model does not fit the data exactly.

Experiments are under way to substantiate the existence of the boundary layer and to determine the layer thickness. Presence of a boundary layer would have a profound effect on the

Figure 21

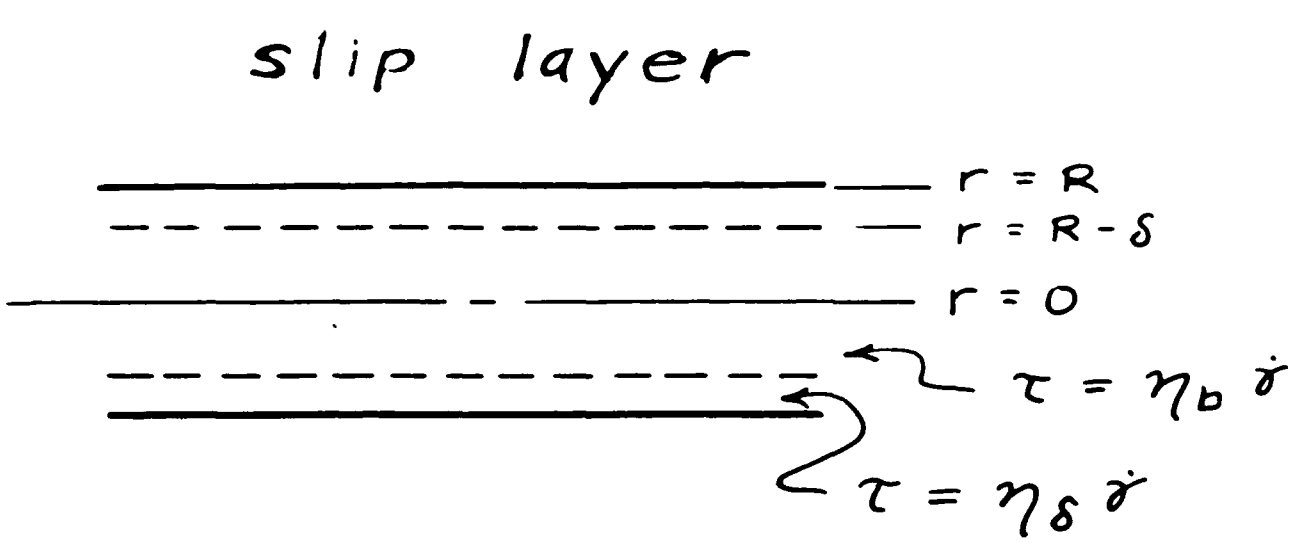

$$\dot{\gamma}_a = \frac{4Q}{\pi R^3}$$

$$\dot{\gamma}_a = \frac{4}{\tau_R^3} \int_0^{\tau_R} \tau \dot{\gamma} \, d\tau$$

assume power-law fluids :

$$\dot{\gamma}_a = \begin{cases} \left(\frac{\tau}{m_0}\right)^{1/n_0}, & 0 < \tau < \tau_{R-\delta}, \text{ core} \\ \left(\frac{\tau}{m_\delta}\right)^{1/n_\delta}, & \tau_{R-\delta} < \tau < \tau_R, \text{ layer} \end{cases}$$

Figure 22

$$\dot{\gamma}_a = 4\left[\left(\frac{n_o m_o^{-1/n_o}}{3n_o+1}\right)\left(1-\frac{\delta}{R}\right)^{3+1/n_o}\tau_R^{1/n_o} + \left(\frac{n_\delta m_\delta^{-1/n_\delta}}{3n_\delta+1}\right)\left(\frac{\delta}{R}\right)^{3+1/n_\delta}\tau_R^{1/n_\delta}\right]$$

$$= \dot{\gamma}_{a,\,core} + \dot{\gamma}_{a,\,layer}$$

$\dot{\gamma}_a$ will show strong R-dependence when

$$\frac{\dot{\gamma}_{a,\,layer}}{\dot{\gamma}_{a,\,core}} >> 1$$

or, when

$$\left(\frac{\delta}{R}\right)^{3+1/n_\delta}\tau_R^{1/n_\delta - 1/n_o} >> 1$$

Figure 23

$n_\delta < n_o$

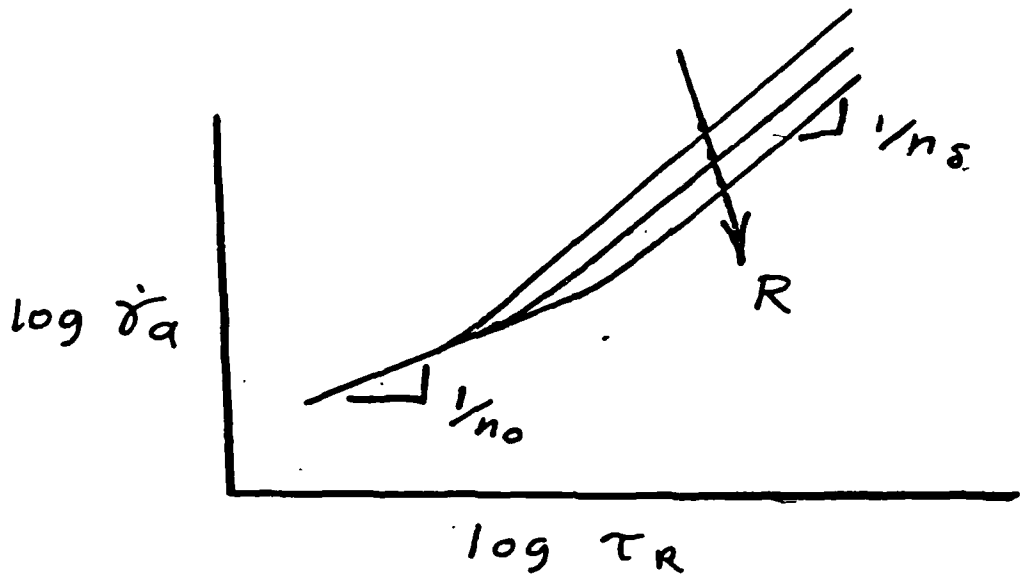

$n_\delta > n_o$

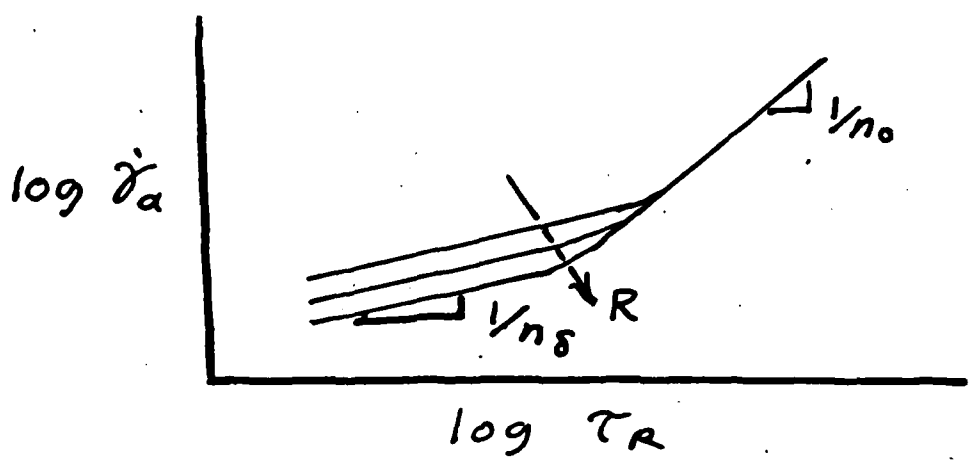

Figure 24

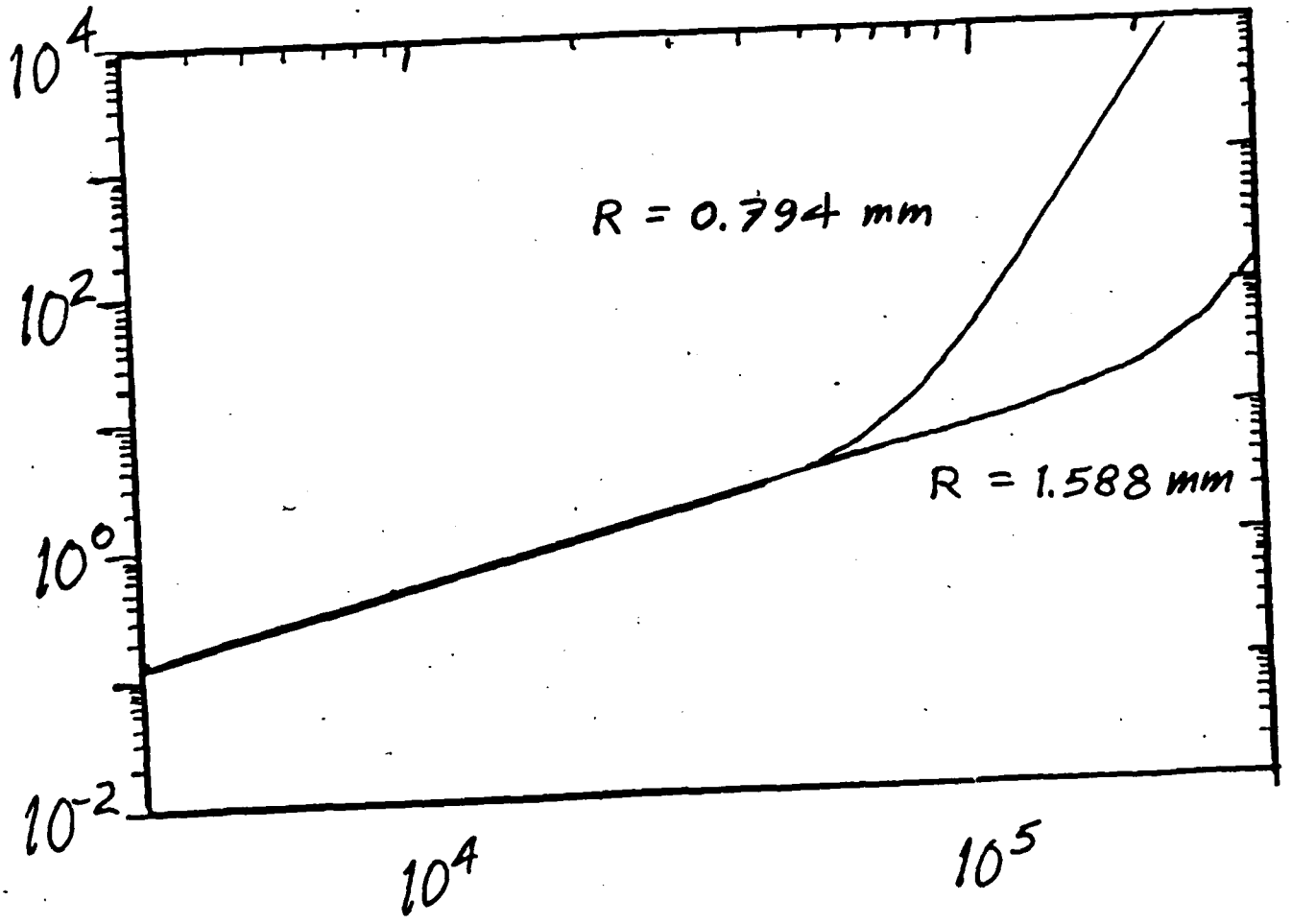

$n_o = 0.9$ $n_s = 0.15$

$m_o \approx 5000\ Pa \cdot s^{0.9}$ $m_s = 200\ Pa \cdot s^{0.15}$

flow through of highly filled polymers through channels. In particular, additional information is required to scale up a flow process for materials with boundary layers.

B. Welding Flows. Experiments and Simulation.

Welding flows occur in many important polymer processing operations. When two streams of molten polymer meet and form a weld interface the macromolecules near the interface can be highly oriented due to flow history. Macromolecules need a long time to diffuse across the interface and to relax to a random configuration.

Several molecular models are available to predict the diffusion across the weld interface. However, they are based on the assumption of randomly coiled molecules on either side of the interface (static welding). The influence of flow-induced orientation on the welding process (dynamic welding) is largely unknown. Moreover, there are few models analysing the kinematics which determine the strain histories and orientations of macromolecules at a weld interface.

Kinematics of ideal flows generated by a thin plate divider in a slit was investigated. A numerical method was used to calculate the stress exhibited by a viscoelastic melt in welding flows. The method assumes that the kinematics are reasonably close to those of a shear-thinning fluid such as Carreau model. The strain history and the resulting stress were calculated via a

tracking method from finite element kinematics. Full-field flow birefringence experiments were done for low-density polyethylene and polystyrene flowing past a thin plate divider in a 1.254-mm planar slit die. By digitally analysing birefringence photographs of the flow field, the birefringence was measured over two dimensions. The birefringence results are in good agreement with stress fields calculated from the numerical simulations. The highest orientation was found in a region surrounding the weld interface just downstream of the plate divider. This orientation relaxed further downstream with the polystyrene relaxing faster than the low-density polyethylene.

III. Prediction of the Mechanical Behavior of Particulate Composites

A. Introduction

The prediction of the mechanical behavior of propellants under thermal or mechanical stresses is of great importance in the effective design of low-vulnerability weapons. The presence of voids due to debonding of oxidizer particles results in significant changes in the burn rate which cannot be tolerated. Prediction of the onset of debonding would allow design of proper processing to avoid this problem.

The method to be presented predicts the stress-strain and dilatational behavior of composites filled with spherical particles and subjected to uniaxial tension. Composite moduli

are calculated, assuming the material acts as a continuum. The laws of linear elasticity are used, with changes in modulus attributed to debonding of filler particles. A brief discussion of the theory used, as well as some calculated results and the experimental work being done follow.

B. Theory

Debonding is the loss of reinforcement due to an adhesive failure between matrix and filler. Debonding produces an ellipsoidal vacuole about the particle which lengthens with increasing strain. The presence of these voids markedly softens and causes large volumetric changes in the material. Several idealized models of the debonding process are being investigated. The simplest model considers the debonded particles to have vanished and the total filler concentration to have decreased correspondingly. Other models include the addition of air to a constant concentration of filler, the replacement of filler particles by air, and a more realistic model which subtracts the reinforcement of the particle while adding a void whose volume increases with strain. The more complex models introduce ambiguities in the calculation of filler concentration since the debonded particles may or may not be considered as part of the total composite volume. Each model requires that the composite modulus be known as a function of the concentration of filler and voids.

Work previously done by J. Farber and R.J. Farris provides the needed relations between concentration and modulus. Their technique makes use of the similarity between the equation of motion for a Newtonian fluid and that of an elastic solid when written in terms of displacements. When the creeping flow approximation is used, there is a term-by-term equivalence. It is therefore apparent that the solution of the equation of motion for the velocity of a Newtonian liquid would also represent the displacement of an elastic solid. Therefore, an expression for the relative viscosity of a suspension would hold for the relative modulus of a composite in the same geometry. When the resulting equation is expressed in incremental form and the increments are made infinitesimal, a differential equation results:

$$\frac{dG}{dc} = \frac{-15G(1 - \nu)(1 - G_i/G)}{[7 - 5\nu + 2(4 - 5\nu)G_i/G])(1 - c)}$$

A similar procedure results in an equation for the bulk modulus:

$$\frac{dK}{dc} \quad \frac{(K_i - K)}{(1 + [(K_i - K)/(K + (4/3)G)])(1 - c)}$$

These nonlinear, coupled differential equations can be solved numerically to give moduli as functions of filler or void volume fraction. The resulting curves agree well with experimental data.

The onset of debonding can be predicted with an energy balance if isotropy is assumed. The loss in mechanical energy due to a decrease in modulus is equated to the energy needed to create two surfaces (that of the particle and that of the void) and the pressure-volume work done in dilating the matrix. If no superimposed pressure is added, the PV work is zero and the energy balance gives the following equation for the strain at which debonding occurs:

$$\epsilon_c = \sqrt{\frac{12\,\gamma}{R\left(\frac{dE}{dc}\right)} - \frac{2P^2\Delta c}{K\left(\frac{dE}{dc}\right)}}$$

where γ is a measure of the energy of adhesion between matrix and filler. The critical strain is inversely proportional to the square root of the particle radius, as has been observed previously by Oberth and others. For a composite of uniform particle size, the calculation of the critical strain at each filler concentration during the debonding process (as defined by the first model described) gives a stress-strain curve with a very sharp yield point, as shown in Figure 25. The inclusion of a particle size distribution gives a more realistic, rounded curve. This model underestimates the dilatation seen in experimental data but gives good qualitative agreement, especially when the simplicity of the model is considered.

Initial work on the more complex three-phase models indicates that the qualitative agreement is significantly improved by the inclusion of voids in the model.

C. Experimental

Preparations are under way to make experimental measurements of stress-strain and dilatation-strain curves on filled polyurethanes. The samples will be prepared from polyfunctional long-chain glycols and toluene diisocyanate, filled with glass beads. Initial work shows that wide varieties of materials can be obtained, ranging from soft rubbers to glassy solids, by varying the fraction of di- and trifunctional glycols used. Current work is concentrating on determining the stoichiometry necessary to compensate for any side reactions present.

The instrument to be used in measuring the stress-strain and dilatational behavior is a high-pressure gas dilatometer, designed by R.J. Farris. The dilatometer measures the differential pressure between selaed chambers containing a deforming sample and a reference volume of air, and relates this pressure difference to the corresponding volume change of the sample using the perfect gas law. The assembly of the dilatometer is nearing completion, and the data acquisition equipment needed should be received early in 1987.

D. Future Work

Future work will include the measurement of stress-strain and dilatation-strain curves on filled polyurethanes of varying matrix properties. Filler concentration, and particle size. Additional work on the debonding models should indicate which model will give the best quantitative agreement with experiment. Additional program refinements will include its extension to include the effects of particle size distribution and superimposed pressures. The theory may be expanded to model different particle shapes and viscoelastic materials.

IV. Collaboration with Industry, DOD and NBS Laboratories

A. Olin

Olin is interested in the manufacturing of LOVA binder. Under the direction of Dr. D. Gavin the synthesis of poly(dioxolane-co-trioxane), PDI, and poly(4-methyl-dioxolane), PMDO, hard and soft segments respectively, have been scaled up. There will soon be sufficiently large quantities of PDT-PMDO TPE for thorough characterizations of chemical, mechanical and rheological properties, heats of combustion and LOVA applications

B. NSWC

Collaboration with Dr. H. Adolph of NSWC has begun. We have performed TGA on 13 polyformal samples. Measurements of their acid sensitivity are underway.

Studies are progressing in the synthesis of liquid crystalline polymers incorporating the polyformals of NSWC.

C. BRL

After Olin had conducted initial extrusion studies on PDT-PMDO TPE with KCl filler and energetic fillers, large samples will be sent to Dr. J. Rocchio of BRL for tests of LOVA performance.

D. Aerojet General

We have begun collaborating with Dr. G. Manzer of Aerojet General. We will synthesize energetic TPE from PDT-PMDO and BAMO. The resulting TPE will be completely characterized.

E. China Lake

Two collaborations will begin this year. We will be working with Dr. R. Yen in the application of magic angle spinning cross polarization NMR to study the basic polymer physics of materials of interest to China Lake.

Samples of PDT, PMDO and their segmented block copolymer TPE will be evaluated for ramjet applications by Dr. G.W. Burdett.

F. NBS

We have begun synthesis of fluorescence probe containing TPE for Dr. F. Wang of NBS to perform rheological measurements.

END

10-87

DTIC